

AperTO - Archivio Istituzionale Open Access dell'Università di Torino

Seep deposits from northern Istria, Croatia: a first glimpse into the Eocene seep fauna of the Tethys region

This is the author's manuscript

Original Citation:

Availability:

This version is available <http://hdl.handle.net/2318/150774> since 2015-09-16T08:48:51Z

Published version:

DOI:10.1017/S0016756814000466

Terms of use:

Open Access

Anyone can freely access the full text of works made available as "Open Access". Works made available under a Creative Commons license can be used according to the terms and conditions of said license. Use of all other works requires consent of the right holder (author or publisher) if not exempted from copyright protection by the applicable law.

(Article begins on next page)

1
2
3
4
5
6
7
8
9
10
11
12
13
14
15
16
17
18
19
20
21
22
23
24
25
26
27
28
29
30
31
32
33
34
35
36
37
38
39
40
41
42
43
44
45
46
47
48
49
50
51
52
53
54
55
56
57
58
59
60

1 Seep deposits from northern Istria, Croatia: a first glimpse into the Eocene seep
2 fauna of the Tethys region

4 M. NATALICCHIO*, J. PECKMANN‡§, D. BIRGEL‡ & S. KIEL¶

6 *Department of Earth Sciences, University of Torino, 10125 Torino, Italy

7 ‡Department of Geodynamics and Sedimentology, Center for Earth Sciences, University of
8 Vienna, 1090 Vienna, Austria

9 ¶Geobiology Group and Courant Centre Geobiology, Geoscience Centre, University of
10 Göttingen, 37077 Göttingen, Germany

12 § Author for correspondence: joern.peckmann@univie.ac.at

14 Keywords: seep fauna, methane-derived carbonates, stable isotopes, biomarkers, Eocene,
15 Istria

17 **Abstract** – Three isolated limestone deposits and their fauna are described from a middle
18 Eocene Flysch succession in northwestern Istria, Croatia. The limestones are identified as
19 ancient methane-seep deposits based on fabrics and characteristic mineral phases, $\delta^{13}\text{C}_{\text{carbonate}}$
20 values as low as -42.2% , and ^{13}C -depleted lipid biomarkers indicative for methane-oxidising
21 archaea. The faint bedding of the largest seep deposit, the great dominance of authigenic
22 micrite over early diagenetic fibrous cement, as well as biomarker patterns indicate that
23 seepage was diffusive rather than advective. Apart from methanotrophic archaea, aerobic
24 methanotrophic bacteria were present at the Eocene seeps as revealed by ^{13}C -depleted
25 lanostanes and hopanoids. The observed corrosion surfaces in the limestones probably reflect

carbonate dissolution caused by aerobic methanotrophy. The macrofauna consists mainly of chemosymbiotic bivalves such as solemyids (*Acharax*), thyasirids (*Thyasira*), and lucinids (*Amanocina*). The middle Eocene marks the rise of the modern seep fauna, but so far the fossil record of seeps of this age is restricted to the North Pacific region. The taxa found at Buje originated during the Cretaceous, whereas taxa typical of the modern seep fauna such as bathymodiolin mussels and vesicomyid clams are absent. Although this is only a first palaeontological glimpse into the biogeography during the rise of the modern seep fauna, it agrees with biogeographic investigations based on the modern vent fauna indicating that the dominant taxa of the modern seep fauna first appeared in the Pacific Ocean.

1. Introduction

Authigenic carbonate rocks forming where methane or oil effuse from the sediments into the bottom waters act as an archive of life in chemosynthesis-based ecosystems at marine seeps (Peckmann & Thiel, 2004; Campbell 2006). The key biogeochemical process at seeps is the anaerobic oxidation of methane (Boetius *et al.* 2000). It results in carbonate precipitation forming seep limestones even way below the carbonate compensation depth (e.g. Ritger *et al.* 1997; Greinert, Bohrmann & Elvert, 2002) and the production of hydrogen sulphide that sustains benthic sulphide-oxidizing bacteria and thiotrophic bacteria in the tissues of chemosymbiotic metazoans (Sibuet & Olu, 1998). A growing number of Phanerozoic seep deposits has been described to date (Campbell, 2006; Teichert & van de Schootbrugge, 2013, and references therein). Their fossil inventory revealed a successive colonisation of seep environments by different groups of metazoans in the course of Earth history, commonly followed by the sooner or later disappearance of these groups of highly specialized taxa.

Methane-seep faunas were first discovered in the early 1980s in the Gulf of Mexico and are now recognized at most continental margins (Paull *et al.* 1984; Baker *et al.* 2010). Their highly specialized taxa are closely related to those at deep-sea hydrothermal vents and many

1
2
3
4
5
6
7
8
9
10
11
12
13
14
15
16
17
18
19
20
21
22
23
24
25
26
27
28
29
30
31
32
33
34
35
36
37
38
39
40
41
42
43
44
45
46
47
48
49
50
51
52
53
54
55
56
57
58
59
60

52 rely on chemotrophic symbionts for nutrition (Paull *et al.* 1985). Although the rise of the
53 modern, mollusc-dominated vent and seep fauna began during the Cretaceous age, the main
54 players at present-day vents and seeps appeared in the early Cenozoic (Campbell & Bottjer,
55 1995; Kiel, 2010; Kiel & Little, 2006; Vrijenhoek, 2013). Biogeographically, however, the
56 Cenozoic fossil record of methane seeps is highly skewed toward the active continental
57 margins of the Pacific Ocean where uplift of deep-water sediments is frequent (Goedert &
58 Squires, 1990; Majima, Nobuhara & Kitazaki 2005; Campbell *et al.* 2008). In contrast, fossil
59 occurrences in the Atlantic realm are restricted to the Caribbean region (Gill *et al.* 2005; Kiel
60 & Peckmann, 2007) and the Mediterranean basin (Taviani, 1994).

61 Here we evaluate the fauna of middle Eocene seep deposits from the northern
62 Mediterranean basin (Istria, Croatia; Venturini *et al.* 1998) in the light of the early evolution
63 of the modern vent and seep fauna, establish the biogeochemical processes that lead to the
64 formation of the seep deposits, describe processes that imprinted their lithology, and
65 reconstruct the composition of fluids and the mode of seepage.

66
67 **2. Geological setting and material**

68 The Istria peninsula, shared by Croatia, Slovenia, and Italy, is bordered to the northeastern
69 Adriatic Sea. During the Eocene, Istria was a part of the Dinaric foreland zone that
70 experienced a strong subsidence in response to the formation of an orogenic wedge (e.g.
71 Živkovic & Babić, 2003). The study area (Fig. 1a, b), located in the Croatian part of
72 northwestern Istria, is characterised by a regional WNW-ESE-oriented anticlinal structure,
73 commonly referred to as the Buje anticline or Buje Karst, whose origin is related to the
74 formation of the Dinarides (Matičec, 1994). At the southern margin of the Buje anticline the
75 foreland sequence is composed by more than 150 m of Lutetian lacustrine to shallow-marine
76 foraminiferal limestones (Drobne & Pavlovec, 1991) and by at least 350 m of Lutetian to
77 Priabonian turbidite deposits (referred to as Flysch Units; Marinčić *et al.* 1996; Pavšić &

Peckmann, 1996; Živković & Babić, 2003) that transgressively overlie an Aptian to Cenomanian sequence of shallow marine carbonates (Venturini *et al.* 1998). The Flysch deposits, in which the studied limestones are enclosed, consist of interbedded siliciclastic sandstones and marlstones as well as rare carbonate megabeds with basal breccias, representing calciturbidites (Venturini *et al.* 1998). The occurrence of turbidites indicates deposition by gravity flows in a deep-sea environment. The majority of the fine-grained marlstones, on the other hand, represents hemipelagic background sedimentation in a basinal setting (Pavšič & Peckmann, 1996). The occurrence of ichnogenera including *Paleodictyon*, as well as foraminifers and ostracods suggests deposition between 700 and 1200 m water depth (Gohrbandt *et al.* 1960; Pavšič & Peckmann, 1996).

The exotic blocks of limestone occurring in the vicinity of the town of Buje (Fig. 1b; 45°24'31''N, 13°40'01''E) have first been described by Venturini *et al.* (1998). The deposits studied here correspond to the “nearby Buje petrol station” section of Venturini *et al.* (1998; their Figures 4 and 5). In the captions of their Figures 10, 11, 13, and 14 as well as Table 1 Venturini *et al.* (1998) refer to this locality as “Buje”. The other two outcrops described by Venturini *et al.* (1998) were no longer accessible during field work in 2011. In the “nearby Buje petrol station” outcrop three limestone bodies are exposed in a road section in the eastern outskirts of Buje (Fig. 2, 3). These deposits are enclosed in a sequence of fine-grained marls intercalated with few decimetre-thick sandstone beds. The lowermost deposit (Buje 1) is about 4 m thick and laterally extends for approximately 20 metres in outcrop, the Buje 2 and 3 deposits are approximately 5 m and 2 m in width and 2 m and 1 m in height, respectively.

99

100 3. Methods

101 Sampling of the carbonate deposits (Buje 1, 2, and 3) has been carried out in spring 2011.
102 Selected samples were prepared for palaeontologic, petrographic, and geochemical
103 investigations. All fossil specimens are deposited in the Geowissenschaftliches Museum,

1
2
3
4
5
6
7
8
9
10
11
12
13
14
15
16
17
18
19
20
21
22
23
24
25
26
27
28
29
30
31
32
33
34
35
36
37
38
39
40
41
42
43
44
45
46
47
48
49
50
51
52
53
54
55
56
57
58
59
60

Georg-August-University Göttingen, Germany (GZG). Thin sections (15 x 10 cm and 10 x 7.5 cm) were studied with transmitted light and cathodoluminescence microscopy using a CITL 8200MK3, operating at about 17 kV and 400 mA. Thin sections were further analysed for their UV-fluorescence on a Nikon microscope with a UV-2A filter block, using ultraviolet light (illumination source 450-490 nm). Scanning electron microscopy and qualitative element recognition were performed with a Cambridge Instruments Stereoscan 360 scanning electron microscope equipped with an energy-dispersive Link System Oxford Instruments microprobe.

For stable isotope analyses mineral phases were drilled from the surface of slabs with a hand-held micro drill. Measurements of carbon and oxygen isotopes were performed with a Finnigan MAT 251 mass spectrometer using the “Kiel” carbonate device type “Bremen“ against natural carbon dioxide from Burgbohl (Rheinland, Germany). A Solnhofen limestone was used as standard, which was calibrated against the international standard NBS 19. Values are reported in the δ -notation relative to Vienna Pee Dee Belemnite (VPDB) standard. Long time standard deviation (1σ) for this measurement was 0.05‰ for $\delta^{13}\text{C}$ and 0.07‰ for $\delta^{18}\text{O}$ values.

Lipid biomarkers were extracted from two carbonate blocks (Buje 1 and 2 deposits), yielding almost identical patterns. Samples were prepared and decalcified as described in Birgel *et al.* (2006a). After saponification with 6% KOH in methanol, the samples were extracted with a microwave extraction system (CEM Discovery) at 80°C and up to 250 W with dichloromethane/methanol (3:1) three times. The resulting extracts were separated into four fractions by column chromatography (500 mg DSC-NH₂ cartridges, Supelco) as described in Birgel *et al.* (2008). Carboxylic acids were measured as their methyl ester (ME) derivatives. All fractions were measured using an Agilent 7890 A GC system coupled to an Agilent 5975 C inert MSD spectrometer. The GC-MS system was equipped with a 30 m HP-5 MS UI fused silica capillary column (0.25 mm i.d., 0.25 μm film thickness). The carrier gas was He. The gas chromatography (GC) temperature program used for both fractions was as

1
2
3 130 follows: 60 °C (1 min); from 60 to 150°C at 10°C/min then to 320°C at 4°/min; 25 min
4
5 131 isothermal. Identification of compounds was based on GC retention times and comparison
6
7 132 with published mass spectra. No separation of crocetane and phytane was achieved with the
8
9 133 used column. The relative abundance of these compounds was assessed by the different
10
11 134 fragmentation patterns, especially by the change of relative abundances of the masses 169
12
13 135 (characteristic for crocetane) and 183 (characteristic for phytane) within the mixed
14
15 136 crocetane/phytane peak. Compound-specific carbon isotope analyses were carried out with a
16
17 137 Thermo Fisher Trace GC Ultra connected via a thermo Fisher GC Isolink interface to a
18
19 138 Thermo Fisher Delta V Advantage spectrometer. GC conditions were identical to those
20
21 139 described above. Carbon isotopes are expressed as $\delta^{13}\text{C}$ values relative to the VPDB standard.
22
23 140 The carbon isotope measurements were corrected for the addition of ME-derivatives. Several
24
25 141 pulses of carbon dioxide with known $\delta^{13}\text{C}$ values at the beginning and the end of the runs
26
27 142 were used for calibration. Instrument precision was checked using a mixture of *n*-alkanes (C_{14}
28
29 143 to C_{40}) with known isotopic composition. The analytical standard deviation was <0.7‰.
30
31
32
33
34
35

145 4. Results

146 4.a. Fauna

147 Microfossils are abundant in the studied carbonate rocks, for the most part being represented
148 by benthic (*Bolivina* sp., *Stilostomella* spp., *Uvigerina* spp., and *Heterolepa* spp.) and planktic
149 (*Turborotalia* sp., *Acarinina* sp. and *Hantkenina* sp.) foraminifera. The occurrence of
150 *Hantkenina* sp. agrees with an Upper Lutetian-Bartonian age (cf. Pavšič & Peckmann, 1996).

151 Macrofossils were found only sporadically in the Buje 1 deposit and were almost absent
152 in the Buje 2 and Buje 3 deposits. Most common is a lucinid bivalve that includes also the
153 largest shell, followed by a thyasirid, and a solemyid bivalve. In addition to these bivalves, a
154 few callianassid claws and other crustacean fragments were found. The bivalves include: (1)
155 two specimens of a solemyid, the larger one 32 mm long and 10 mm high with the anterior

1
2
3
4
5
6
7
8
9
10
11
12
13
14
15
16
17
18
19
20
21
22
23
24
25
26
27
28
29
30
31
32
33
34
35
36
37
38
39
40
41
42
43
44
45
46
47
48
49
50
51
52
53
54
55
56
57
58
59
60

end missing. It shows an elongate S-shaped band extending from the posteroventral corner of the anterior adductor muscle scar to the dorsal shell margin, had an external ligament, and is therefore referred to as *Acharax* (Fig. 4a-c). (2) Two specimens of a *Nucula*; the larger one is 20 mm long and 15 mm high, and although the taxodont hinge is missing in these specimens, they have the general shape of a *Nucula* and show the radial striation and crenulate ventral margin common to this genus (Fig. 4d). (3) Four specimens belong to *Thyasira* due to their general shape and strong posterior sulcus (Fig. 4e); the largest is 40 mm long. The “undetermined Veneroida (?Kelliidae)” figured by Venturini *et al.* (1998, p. 225, Fig. 11) may also belong to this *Thyasira* species. (4) Seven specimens and fragments of an oval lucinid bivalve with an edentulous, narrow hinge without triangular excavation below the umbo, and a maximum length of 52 mm (Fig. 4f-j) belong to the genus *Amanocina*. The lucinid is most likely the same species as the “*Lucina*” figured by Venturini *et al.* (1998, p. 225, Fig. 10).

4.b. Petrography and stable isotopes

The lithology of the three Buje carbonate deposits (Buje 1 to 3) is quite similar. The limestones consist of fossiliferous and bioturbated mudstone and wackestone (Fig. 5). The matrix is made up of dark brown micrite, revealing a bright autofluorescence (Fig. 6a, b). Terrigenous particles are angular, including abundant quartz and rare feldspar grains as well as lithic clasts. Apart from detrital grains, the micritic matrix contains abundant biogenic detritus, mostly tests of foraminifera (Fig. 6c). Some mm to cm wide, irregular cavities occur; the cavities are interpreted to result from bioturbation, representing successively filled burrows. Some cavities show geopetal infill (Fig. 6d). The cavities are filled by sediment and authigenic phases including peloids, homogenous micrite, laminated micrite, a phase referred to as cauliflower micrite, and different generations of carbonate cements (Fig. 6d-f). Peloidal fabrics are particularly abundant (Fig. 6e). They consist of ovoidal peloids, showing an intense fluorescence, surrounded by a non-fluorescent calcite microspar. On the basis of shape and

182 composition, peloids are interpreted to represent faecal pellets. Banding in the authigenic,
 183 laminated micrites is sub-parallel to cavity walls (Fig. 6e). In places the laminated micrite is
 184 broken to pieces, forming fragments surrounded by calcite cement.

185 The cauliflower micrite is an obviously authigenic variety of micrite found in some of the
 186 cavities. It is represented by aggregates of mottled, microcrystalline calcite (Fig. 7a, b). Its
 187 aggregates exhibit a domal, grooved shape, resembling cauliflower. Micron-sized irregular
 188 pores, filled by calcite microspar, are present within these domes, generating a sponge-like
 189 texture (Fig. 7c). The fluorescent cauliflower micrite (Fig. 7d) is commonly covered by a
 190 circumgranular calcite cement (Fig. 7b, c). Remaining porosity in the cavities was
 191 subsequently filled by two main generations of cement, (1) banded and botryoidal aggregates
 192 of fibrous aragonite cement, mostly recrystallized to calcite, and (2) a drusy mosaic of equant
 193 calcite cement (Fig. 6c-f). Carbonate cements are overall not abundant, being restricted to the
 194 cavities believed to result from bioturbation.

195 The micritic matrix of the Buje deposits records episodes of carbonate corrosion. The
 196 surfaces of the affected aggregates of micrite are highly irregular, and commonly covered by a
 197 black rim of an opaque mineral up to a few tens of μm in thickness (Fig. 8a, b). Backscatter
 198 and EDS observations revealed that these rims consist of scattered bright grains (Fig. 8c)
 199 characterized by high contents of iron and manganese.

200 The volumetrically dominant micrite of the Buje carbonates has been analysed for its
 201 stable carbon and oxygen isotope composition; the amount of banded and botryoidal cement
 202 was not sufficient to allow for isotope analysis. The $\delta^{13}\text{C}$ values of micrite range from -42.2
 203 to -22.7‰ , the corresponding $\delta^{18}\text{O}$ values range from -3.9 to 0.0‰ (Fig. 9). The Buje 1
 204 deposit revealed the most negative $\delta^{13}\text{C}$ and $\delta^{18}\text{O}$ values, as low as -42.2 and -3.9‰ ,
 205 respectively, with most $\delta^{13}\text{C}$ values falling between -35.2 and -30.2‰ . Buje 2 and Buje 3
 206 deposits show overall similar isotope values with less ^{13}C and ^{18}O depletion compared to the
 207 Buje 1 deposit.

208

209 **4.c. Biomarkers**

210 Hydrocarbons, carboxylic acids, and alcohols were analysed. However, lipid biomarkers in
211 the alcohol fraction are only poorly preserved, and are thus not useful for the interpretation of
212 the depositional environment. The major group of compounds in the hydrocarbon fraction are
213 isoprenoid hydrocarbons (Fig. 10a). Among them are the head-to-tail linked isoprenoid
214 phytane (approximately 60% of the combined peak) and the tail-to-tail linked isoprenoid
215 crocetane (approximately 40%); their combined peak is the highest peak in this fraction. The
216 next abundant isoprenoids are the tail-to-tail linked isoprenoid pentamethylicosane (PMI) and
217 the head-to-head linked isoprenoid biphytane (bp-0). Other, minor constituents are
218 monocyclic biphytane (bp-1) with one cyclopentane ring and the tail-to-tail linked isoprenoid
219 squalane, as well as the head-to-tail linked isoprenoid pristane. Other than isoprenoids, few
220 straight-chain *n*-alkanes are present. Their overall distribution is patchy with the exception of
221 *n*-C₂₃, resembling the inventory of modern and ancient, non-oil stained seep carbonates and
222 sediments (e.g. Thiel *et al.* 2001; Peckmann *et al.* 2007; Chevalier *et al.* 2013). Apart from
223 aliphatic lipid biomarkers, few cyclic compounds, mainly steranes and one hopanoid were
224 found. Among steroids, most abundant are C₂₈ and C₂₉ steranes. Other detected steroids are
225 lanostanes, which have been described in some seep carbonates (Birgel & Peckmann, 2008).
226 The most abundant cyclic terpenoid found is the hopanoid hop-17(21)-ene.

227 The isoprenoids have the most negative $\delta^{13}\text{C}$ values with -111‰ and -109‰ for PMI
228 and bp-0, respectively. The head-to-tail linked isoprenoid pristane (-60‰) and the *n*-alkane
229 *n*-C₂₃ (-66‰) revealed intermediate values (Fig. 9), whereas other short-chain *n*-alkanes are
230 significantly less ^{13}C -depleted (-34‰). The $\delta^{13}\text{C}$ values of steranes fall in the same range as
231 short-chain and long-chain *n*-alkanes. Lanostanes are more ^{13}C -depleted with an average
232 value of -47‰ . Hop-17(21)-ene is more ^{13}C -depleted (-64‰) than the lanostanes.

233 The carboxylic acid fraction is predominated by *n*-fatty acids ranging from C₁₄ to C₂₈
 234 (Fig. 10b). The fatty acids are characterized by an overall even-over-odd predominance.
 235 Highest contents were found for short-chain *n*-C₁₆ fatty acid. Other abundant compounds are
 236 *n*-C₁₆ and C₁₈ fatty acids with one double bond. Apart from *n*-fatty acids, terminally-branched
 237 fatty acids are abundant, especially those comprising 15 carbons. Other compounds in the
 238 carboxylic acid fraction are phytanoic acid and PMI acid. Phytanoic acid co-elutes with a
 239 C_{18:1} fatty acid. Only one hopanoic acid, 17β(H),21β(H)-bishomohopanoic acid, was
 240 identified.

241 The strongest ¹³C depletions in the carboxylic acids were found for the isoprenoid PMI
 242 acid (−107‰). Although combined with the isotopic signature of the co-eluting *n*-C_{18:1} fatty
 243 acid, phytanoic acid is still considerably ¹³C-depleted (−75‰). Other compounds with
 244 significant depletion in ¹³C are the terminally-branched *iso*- and *anteiso*-C₁₅ fatty acids with
 245 δ¹³C values of −68‰ and −82‰, respectively, as well as 17β(H),21β(H)-bishomohopanoic
 246 acid (−70‰). Short-chain *n*-fatty acids yielded values of around −50‰, whereas the long-
 247 chain fatty acids revealed higher values (average −31‰).

249 5. Discussion

250 5.a. Biogeographic and evolutionary aspects

251 Methane seepage and associated faunal communities in the Mediterranean realm are known
 252 from the late Mesozoic when large lucinid bivalves and rhynchonellide brachiopods inhabited
 253 cold seeps along the northern shore of the Tethys Ocean (Gaillard, Rio & Rolin, 1992;
 254 Campbell & Bottjer, 1995; Peckmann *et al.* 1999; Kiel, 2013) and from the Miocene onward,
 255 largely along the Apennine chain in Italy (Ricci Lucchi & Vai, 1994; Taviani, 2011). These
 256 Neogene seep deposits are generally referred to as ‘Calcarei a *Lucina*’ (Clari *et al.* 1988;
 257 Taviani, 1994). Among them, the Miocene deposits contain essentially a modern seep fauna

1
2
3
4
5
6
7
8
9
10
11
12
13
14
15
16
17
18
19
20
21
22
23
24
25
26
27
28
29
30
31
32
33
34
35
36
37
38
39
40
41
42
43
44
45
46
47
48
49
50
51
52
53
54
55
56
57
58
59
60

consisting of large bathymodiolin, vesicomysid, and lucinid bivalves, while the few Pliocene examples appear to have a reduced character of the modern Mediterranean Sea seep fauna (Table 1; Taviani, 2014). Many of the taxa that inhabit vents and seeps today originated in the early Cenozoic (Kiel & Little, 2006; Amano & Kiel, 2007; Kiel & Amano, 2013; Vrijenhoek, 2013). The middle Eocene Buje deposits can thus provide insights into the early evolution of the seep fauna and its biogeography.

The only seep deposits coeval with the Buje seeps are those of the middle Eocene Humptulips Formation in western Washington State, USA, and thus from the Pacific realm (Goedert & Squires, 1990). They share the common solemyids, the large thysirids, and the edentulous lucinids, although the latter are represented by different genera in the two regions (cf. Goedert & Squires, 1990; Saul, Squires & Goedert, 1996; Kiel, 2013). The Humptulips seep deposits differ, however, by the presence of large, high spired gastropods (Goedert & Kaler, 1996; Kiel, 2008) and vesicomysid bivalves (Squires & Goedert, 1991; Amano & Kiel, 2007), which appear to be absent from the Buje deposits. The Humptulips limestones also include the earliest bathymodiolin mussels discovered so far (Kiel & Amano, 2013). From one of the seep deposits at Buje, Venturini *et al.* (1998) reported several specimens of the mytilid ‘*Modiolus*’ that could potentially represent an as-yet unidentified bathymodiolin mussel; unfortunately that particular deposit was no longer accessible during our field work and the identity of this mussel remains elusive. The fauna of the Buje seep deposits is only a first glimpse into the Eocene seep fauna of the central Tethys Ocean and is unlikely to represent the full diversity of the regional pool of seep-inhabiting taxa. However, if taken at face value, the absence of the main modern taxa (bathymodiolins and vesicomysids) from Buje at a time when these taxa were present at Pacific seeps is in agreement with molecular phylogenetic analyses (Lorion *et al.* 2013; Roterman *et al.* 2013; Stiller *et al.* 2013) and quantitative biogeographic analyses (Bachraty *et al.* 2009; Moalic *et al.* 2012), which indicate a Pacific origin of the modern vent and seep fauna.

Compared to the ‘Calcarei a *Lucina*’ seep deposits in the Italian Miocene (Fig.1a; Clari *et al.* 1994; Taviani, 1994) and the modern Mediterranean seep fauna (Olu-Le Roy *et al.* 2004; Ritt *et al.* 2010; Taviani *et al.* 2013), the middle Eocene seep fauna at Buje shows clear differences (Table 1). Solemyids are rare in the Neogene to modern seeps in the Mediterranean Sea (Taviani *et al.* 2011; Rodrigues, Duperron & Gaudron 2011) in contrast to Buje, where they are common. Also the large *Thyasira* is a distinctive feature of the Buje seeps, while thyasirids are absent from the ‘Calcarei a *Lucina*’ deposits (Taviani, 2011; S. Kiel, own observation), and in the modern Mediterranean seep fauna they are represented only by a small (~10 mm) species (Olu-Le Roy *et al.* 2004). The lucinids at the Miocene to modern Mediterranean seeps clearly belong to different genera than the lucinid at Buje (Olu-Le Roy *et al.* 2004; Taviani, 2011; Kiel & Taviani, unpub. data), which belongs to the widespread Early Cretaceous to Oligocene genus *Amanocina*.

5.b. Microbial activity steering carbonate formation and destruction

The Buje carbonate deposits show several petrographical and geochemical lines of evidence that agree with a microbial origin sustained by hydrocarbon seepage. Not only the negative $\delta^{13}\text{C}$ values as low as -42‰ agree with methane seeping (cf. Paull *et al.* 1992; Peckmann & Thiel, 2004), but also microfabrics, such as peloidal and clotted micrite, laminated micrite, and banded and botryoidal cement filling cavities are typical of seep carbonates (e.g. Peckmann & Thiel, 2004). Finally, lipid biomarkers characteristic for methane seepage are found in the Buje deposits, confirming their microbial origin resulting from methane oxidation. Among the observed compounds, the most ^{13}C -depleted acyclic isoprenoids such as mixed phytane/croctane (-98‰), PMI (-111‰), and acyclic biphytane (-109‰) are molecular fossils of methanotrophic archaea (e.g. Elvert, Suess & Whiticar, 1999; Peckmann & Thiel, 2004; Birgel *et al.* 2006a; Peckmann, Birgel & Kiel, 2009). These biomarkers are accompanied by molecular fossils of sulphate-reducing bacteria, such as *iso*- and *anteiso*- C_{15}

1
2
3
4
5
6
7
8
9
10
11
12
13
14
15
16
17
18
19
20
21
22
23
24
25
26
27
28
29
30
31
32
33
34
35
36
37
38
39
40
41
42
43
44
45
46
47
48
49
50
51
52
53
54
55
56
57
58
59
60

fatty acids (Elvert *et al.* 2003; Birgel *et al.* 2006b). As commonly observed in seep deposits, the lipids of the sulphate-reducing bacteria involved in anaerobic oxidation of methane are less ¹³C-depleted (−82‰ for *anteiso*-C₁₅ FA) than the lipids of methanotrophic archaea (e.g. Peckmann & Thiel, 2004).

At first glance, the petrographical characteristics and stable isotope and lipid biomarker patterns of the Buje deposits are not much different from other ancient Mediterranean seep deposits (e.g. Peckmann *et al.* 2004; Clari *et al.* 2009; Natalicchio *et al.* 2013). However, the Buje seep deposits show some peculiarities, as for example the occurrence of cauliflower micrite. These dome-shaped precipitates are made up of fluorescent clotted micrite and formed *in-situ* within cavities, properties that typify the products of organomineralisation (cf. Reitner *et al.* 1995; Dupraz *et al.* 2009). Two possible modes of formation are envisaged, (1) mineralised microbial mats or (2) sponges. (1) Mineralized biofilms have already been documented in Eocene seep deposits from western Washington State (Peckmann *et al.* 2003) and in Miocene seep deposits from the Italian Apennine (Peckmann *et al.* 1999). The cauliflower shape, representing a domal, accretionary mode of growth on a mm to cm scale in a cryptic environment is different from previous reports of much thinner mineralised biofilms within cracks of preexisting seep carbonate. Based on the larger size of the Buje cauliflower micrite and its domal growth habit along with its intense autofluorescence it seems feasible that this micrite resulted from the mineralisation of microbial mats that performed anaerobic oxidation of methane. The validity of this scenario is enforced by the presence of subsurface microbial mats of anaerobic oxidation of methane-performing prokaryotes at active seeps in the Black Sea (Treude *et al.* 2005). (2) Alternatively, the domal growth, clotted microfabric, and reticulate porosity of the cauliflower micrite resembles the outcome of sponge taphonomy (e.g. Delecat *et al.* 2001). Because no spicules have been observed, it is unlikely that cauliflower micrite represents fossils of spicular sponges. Even in case of siliceous spicules, the spicules would have been probably preserved in the authigenic seep carbonate. Where

sponges have been reported in ancient seep deposits, their overall preservation including spicules was good in case of Mesozoic examples (Peckmann *et al.* 1999) and excellent in case of Cenozoic examples (Goedert & Squires, 1990; Rigby & Goedert, 1996). If the sponge interpretation is correct, the sponges were probably non-spicular, belonging to a group informally referred to as keratose demosponges (J. Reitner, pers. comm.). Despite of lacking spicules, the taphonomy of keratose sponges results in micritic carbonate fabrics that can still be recognized in Phanerozoic rocks (Luo & Reitner, 2014). Seep-dwelling sponges have been reported from a number of modern sites (Olu-Le Roy *et al.* 2004, and references therein). Some demosponges have even been shown to contain endosymbiotic methanotrophic bacteria (Vacelet *et al.* 1996; Olu-Le Roy *et al.* 2004; Baco *et al.* 2010).

The abundant irregular corrosion surfaces partially covered by iron and manganese precipitates indicate dissolution of carbonate. Such dissolution features coupled with iron and manganese enrichment have commonly been interpreted as the product of microbially-driven corrosion, as for example reported for reef carbonates (Reitner *et al.* 2000; Tribollet *et al.* 2011). Analogous features have also been observed in ancient (Campbell *et al.* 2002; Peckmann *et al.* 2003; Birgel *et al.* 2006b) and modern (Matsumoto, 1990; Himmler *et al.* 2011) seep carbonates and were interpreted as biologically-induced corrosion features as well. Matsumoto (1990) was the first to suggest that carbonate corrosion at seeps is driven by bacterial aerobic methane oxidation and sulphide oxidation. Both processes have the potential to lower the pH and may thus promote carbonate dissolution (Himmler *et al.* 2011; Tribollet *et al.* 2011). Molecular fossils of sulphide-oxidizing bacteria cannot be easily identified in ancient rocks, since these lipids are of low specificity and prone to degradation (cf. Arning *et al.* 2008). In contrast, the former presence of aerobic methanotrophs at seeps can be constrained by lipid biomarkers including lanostanes and some hopanoids (Peckmann *et al.* 1999; 2004; Birgel & Peckmann, 2008; Sandy *et al.* 2012). The low $\delta^{13}\text{C}$ values of lanostanes and hopanoids in the Buje limestones agree with aerobic methanotrophs as source organisms,

1
2
3
4
5
6
7
8
9
10
11
12
13
14
15
16
17
18
19
20
21
22
23
24
25
26
27
28
29
30
31
32
33
34
35
36
37
38
39
40
41
42
43
44
45
46
47
48
49
50
51
52
53
54
55
56
57
58
59
60

although other sources cannot be excluded in case of the ¹³C-depleted hopanoids (cf. Blumenberg *et al.* 2006; Eickhoff *et al.* 2013). The potential of aerobic methanotrophs to cause carbonate dissolution has recently been proven in laboratory experiments (Krause *et al.* 2014). Based on the confirmation that this mechanism is indeed capable of inducing carbonate dissolution and the detection of molecular fossils of aerobic methanotrophs, carbonate corrosion archived in the Buje seep limestones is best explained by aerobic methanotrophy.

5.c. Constraints on fluid flow

The occurrence of both anaerobic oxidation of methane – as revealed by ¹³C-depleted biomarkers and ¹³C-depleted authigenic carbonates – and aerobic oxidation of methane – as revealed by ¹³C-depleted biomarkers and carbonate corrosion – indicates discontinuous oxygenation conditions in the subsurface close to the seafloor at the Buje seep sites. The precipitation of the ¹³C-depleted micrite driven by anaerobic oxidation of methane occurred in anoxic environments within the pore space of the detrital background sediment, leading to the occlusion of the sedimentary matrix. After the pore space was successively filled by micrite, carbonate precipitation was largely restricted to some cavities resulting from preceding bioturbation, and allowing for the formation of fibrous, banded and botryoidal aragonite cement and clotted micrite. Based on the evidence for carbonate corrosion and the preservation of diagnostic biomarkers, at least some of the aerobic methanotrophic bacteria most probably lived in oxic sediments, rendering unlikely that these biomarkers were exclusively sourced from bacteria dwelling in the water column above the seeps.

A set of observations indicates that the mode of seepage was diffusive rather than advective. The Buje seep limestones largely consist of authigenic micrite cementing background sediments. Such a pattern with the dominance of micrite over early diagenetic aragonite cements is typical for diffusive seepage (e.g. Peckmann, Birgel & Kiel, 2009; Haas *et al.* 2010). Similarly, the faint stratification apparent in the Buje 1 deposit is an additional

argument in favour of this interpretation. Similarly, the circumstance that biphytane occurs in much higher contents than crocetane agrees with the dominance of archaea of the so-called ANME-1 group (Blumenberg *et al.* 2004; Niemann & Elvert, 2008; Rossell *et al.* 2011), another observation in favour of diffusive seepage (Nauhaus *et al.* 2005; Peckmann, Birgel & Kiel, 2009). ANME-1 archaea, like ANME-2 archaea, are commonly associated with sulphate-reducing bacteria of the *Desulfosarcina/Desulfococcus* branch of the Deltaproteobacteria (Knittel & Boetius, 2009). The bacterial partners of the ANME-1 archaea can be discerned from those of ANME-2 archaea by a much higher proportion of *ai*-C₁₅ fatty acid (Blumenberg *et al.* 2004; Niemann & Elvert, 2008), a compound that is particularly abundant in the Buje limestones (see Fig. 10b). All these observations argue in favour of diffusive seepage. It should, however, be kept in mind that other factors than just seepage activity can influence the distribution of ANME-1 versus ANME-2 archaea and the abundance of aerobic methanotrophs as well. An obvious factor for example is temperature, whereby higher temperatures are known for favour ANME-1 over ANME-2 archaea (Nauhaus *et al.* 2005).

It is interesting to note that some Cretaceous seep deposits for which diffusive seepage has been envisaged contain biomarkers of aerobic methanotrophs as well (Peckmann, Birgel & Kiel, 2009; Sandy *et al.* 2012), although the majority of seep deposits lacks these compounds (e.g. Peckmann & Thiel, 2004). Because the sulphate-methane transition zone (SMTZ) tends to be situated deeper within the sediments at sites of diffusive seepage than at sites of advective seepage (e.g. Sahling *et al.* 2002; Luff & Wallmann, 2003), we suggest that the preservation of lipids of aerobic methanotrophs is favoured in limestones forming at seeps typified by diffusive seepage – this is not meant to say that aerobic methanotrophs are necessarily more abundant at diffusive seeps. With aerobic methanotrophy being able to extend to greater sediment depth at diffusive seeps, the likelihood probably increases that the lipids of aerobic methanotrophs become engulfed in authigenic seep carbonates at a later stage

1
2
3
4
5
6
7
8
9
10
11
12
13
14
15
16
17
18
19
20
21
22
23
24
25
26
27
28
29
30
31
32
33
34
35
36
37
38
39
40
41
42
43
44
45
46
47
48
49
50
51
52
53
54
55
56
57
58
59
60

upon dilatation of the zone of anaerobic oxidation of methane. If seepage continues for extended periods of time – as envisaged for the thick Buje 1 deposit – the prolonged formation of methane-derived carbonates, thus, assures the preservation of process markers of those biogeochemical processes that occurred in close proximity of the strata affected by anaerobic oxidation of methane. This effect will be intensified upon variations of seepage intensity that allow for vertical displacement of the SMTZ (cf. Feng, Chen & Peckmann, 2009). An upward movement of the SMTZ caused by an increase of seepage intensity and accompanied by a shift of carbonate formation to shallower depth will particularly favour the preservation of the lipids of aerobic methanotrophs.

6. Conclusions

The fossil record and molecular age estimates indicate that the dominant taxa of the modern vent and seep fauna appeared during the Eocene. The fossil record of seep communities of this age, however, is highly skewed toward the Pacific region and thus macrofauna of the Buje seep deposits provides a first glimpse into the seep fauna of the Tethyan region. The absence of the main modern taxa (bathymodiolin mussels and vesicomid clams) from the Buje seeps agrees with other lines of evidence suggesting that the modern vent and seep fauna originated in the Pacific Ocean. The Buje seep fauna also indicates a dynamic evolution of seep faunas in the Tethyan/Mediterranean basin: it resembles Cretaceous to early Palaeogene seep faunas from other parts of the world, whereas the late Miocene ‘*Calcar* a *Lucina*’ fauna in Italy resembles other Miocene to modern seep faunas worldwide, and the Pliocene seep faunas from northern Italy have the somewhat restricted character of Mediterranean seep fauna today that probably resulted from the extinction of the more ‘oceanic’ Miocene seep faunas during the Messinian salinity crisis.

The Buje seep deposits formed as a consequence of anaerobic oxidation of methane as revealed by the presence of ¹³C-depleted biomarkers of methanotrophic archaea and

associated sulphate-reducing bacteria. Apart from these anaerobic prokaryotes, aerobic methanotrophic bacteria lived at the middle Eocene seeps. Their metabolism apparently led to a local decrease of pore water pH values, which resulted in the dissolution of carbonate minerals. The large size of the Buje 1 deposit suggests that seepage activity was long-lasting. (1) Its faint stratification, (2) the dominance of authigenic micrite over early diagenetic fibrous cement, (3) biomarker patterns of the prokaryotes performing anaerobic oxidation of methane, and (4) possibly the preservation of the lipids of aerobic methanotrophs indicate that seepage activity was mostly diffusive rather than advective.

Acknowledgements. We thank Leopold Slawek (Vienna, Austria) for thin section preparation, Gerhard Hundertmark (Göttingen, Germany) for photography, Monika Segl (Bremen, Germany) for carbon and oxygen isotope analysis of carbonate samples, Birgit Wild and Andreas Richter (both Vienna, Austria) for help with compound-specific carbon isotope measurements, Joachim Reitner (Göttingen, Germany) for comments on keratose sponges, and two anonymous referees for comments that helped improving the manuscript. Financial support was provided by the Deutsche Forschungsgemeinschaft through grant Ki802/6-1 to SK.

References

- ARNING, E.T., BIRGEL, D., SCHULZ-VOGT, H.N., HOLMKVIST, L., JØRGENSEN, B.B., LARSSON, A. & PECKMANN, J. 2008. Lipid biomarker patterns of phosphogenic sediments from upwelling regions. *Geomicrobiology Journal* **25**, 69–82.
- AMANO, K. & KIEL, S. 2007. Fossil vesicomid bivalves from the North Pacific region. *The Veliger* **49**, 270–293.
- BACHRATY, C., LEGENDRE, P. & DESBRUYÈRES, D. 2009. Biogeographic relationships among deep-sea hydrothermal vent faunas at global scale. *Deep-Sea Research I* **56**, 1371–1378.
- BACO, A.R., ROWDEN, A.A., LEVIN, L.A., SMITH, C.R. & BOWDEN, D.A. 2010. Initial characterization of cold seep faunal communities on the New Zealand Hikurangi margin. *Marine Geology* **272**, 251–259.
- BAKER, M.C., RAMIREZ-LLODRA, E., TYLER, P.A., GERMAN, C.R., BOETIUS, A., CORDES, E.E., DUBILIER, N., FISHER, C.R., LEVIN, L.A., METAXAS, A., ROWDEN, A.A., SANTOS, R.S.,

- SHANK, T.M., VAN DOVER, C.L., YOUNG, C.M. & WARÉN, A. 2010. Biogeography, ecology, and vulnerability of chemosynthetic ecosystems in the deep sea. In: A. McIntyre (Editor), *Life in the World's Oceans: Diversity, Distribution, and Abundance*. Wiley-Blackwell, pp. 161–182.
- BARBIERI, R. & CAVALAZZI, B. 2005. Microbial fabrics from Neogene cold seep carbonates, Northern Apennine, Italy. *Palaeogeography, Palaeoclimatology, Palaeoecology* **227**, 143–155.
- BIRGEL, D. & PECKMANN, J. 2008. Aerobic methanotrophy at ancient marine methane seeps: a synthesis. *Organic Geochemistry* **39**, 1659–1667.
- BIRGEL, D., PECKMANN, J., KLAUTZSCH, S., THIEL, V. & REITNER, J. 2006b. Anaerobic and aerobic oxidation of methane at Late Cretaceous seeps in the Western Interior Seaway, USA. *Geomicrobiology Journal* **23**, 565–577.
- BIRGEL, D., THIEL, V., HINRICHS, K.-U., ELVERT, M., CAMPBELL, K.A., REITNER, J., FARMER, J.D. & PECKMANN, J. 2006a. Lipid biomarker patterns of methane-seep microbialites from the Mesozoic convergent margin of California. *Organic Geochemistry* **37**, 1289–1302.
- BIRGEL, D., ELVERT, M., HAN, X. & PECKMANN, J. 2008. ¹³C-depleted biphytanic diacids as tracers of past anaerobic oxidation of methane. *Organic Geochemistry* **39**, 152–156.
- BLUMENBERG, M., SEIFERT, R., REITNER, J., PAPE, T. & MICHAELIS, W. 2004. Membrane lipid patterns typify distinct anaerobic methanotrophic consortia. *Proceedings of the National Academy of Sciences of the United States of America* **101**, 11111–11116.
- BLUMENBERG, M., KRÜGER, M., NAUHAUS, K., TALBOT, H.M., OPPERMAN, B.I., SEIFERT, R., PAPE, T. & MICHAELIS, W. 2006. Biosynthesis of hopanoids by sulphate-reducing bacteria (genus *Desulfovibrio*). *Environmental Microbiology* **8**, 1220–1227.
- BOETIUS, A., RAVENSCHLAG, K., SCHUBERT, C.J., RICKERT, D., WIDDEL, F., GIESEKE, A., AMANN, R., JØRGENSEN, B.B., WITTE, U. & PFANNKUCHE, O. 2000. A marine microbial consortium apparently mediating anaerobic oxidation of methane. *Nature* **407**, 623–626.
- CAMPBELL, K.A. 2006. Hydrocarbon seep and hydrothermal vent paleoenvironments and paleontology: Past developments and future research directions. *Palaeogeography, Palaeoclimatology, Palaeoecology* **232**, 362–407.
- CAMPBELL, K.A. & BOTTJER, D.J., 1995. *Peregrinella*: an Early Cretaceous cold-seep-restricted brachiopod. *Paleobiology* **24**, 461–478.
- CAMPBELL, K.A., FARMER, J.D. & DES MARAIS, D. 2002. Ancient hydrocarbon seeps from the Mesozoic convergent margin of California: carbonate geochemistry, fluids and palaeoenvironments. *Geofluids* **2**, 63–94.
- CAMPBELL, K.A., FRANCIS, D.A., COLLINS, M., GREGORY, M.R., NELSON, C.S., GREINERT, J. & AHARON, P. 2008. Hydrocarbon seep-carbonates of a Miocene forearc (East Coast Basin), North Island, New Zealand. *Sedimentary Geology* **204**, 83–105.
- CHEVALIER, N., BOULOUBASSI, I., BIRGEL, D., TAPHANEL, H.-M. & LÓPEZ-GARCÍA, P. 2013. Microbial methane turnover at Marmara Sea cold seeps: a combined 16S rRNA and lipid biomarker investigation. *Geobiology* **11**, 55–71.
- CLARI, P.A., GAGLIARDI, C., GOVERNA, M.E., RICCI, B. & ZUPPI, G.M. 1988. I Calcari di Marmorito: una testimonianza di processi diagenetici in presenza di metano. *Bollettino del Museo Regionale di Scienze Naturali di Torino* **5**, 197–216.
- CLARI, P., FORNARA, L., RICCI, B. & ZUPPI, G.M. 1994. Methane-derived carbonates and chemosymbiotic communities of Piedmont (Miocene, northern Italy): An update. *Geo-Marine Letters* **14**, 201–209.
- CLARI, P., PIERRE, F., DELA, MARTIRE, L. & CAVAGNA, S. 2009. The Cenozoic CH₄-derived carbonates of Monferrato (NW Italy): A solid evidence of fluid circulation in the sedimentary column. *Marine Geology* **265**, 167–184.

- CONTI, S. & FONTANA, D. 1999. Miocene chemohierms of the northern Apennines, Italy. *Geology* **27**, 927–930.
- CONTI, S. & FONTANA, D. 2005. Anatomy of seep-carbonates: Ancient examples from the Miocene of the northern Apennines (Italy). *Palaeogeography, Palaeoclimatology, Palaeoecology* **227**, 156–175.
- DELA PIERRE, F., MARTIRE, L., NATALICCHIO, M., CLARI, P. & PETREA, C. 2010. Authigenic carbonates in Upper Miocene sediments of the Tertiary Piedmont Basin (NW Italy): Vestiges of an ancient gas hydrate stability zone? *Geological Society of America Bulletin* **122**, 994–1010.
- DELECAT, S., PECKMANN, J. & REITNER, J. 2001. Non-rigid cryptic sponges in oyster patch reefs (Lower Kimmeridgian, Langenberg/Oker, Germany). *Facies* **45**, 231–254.
- DROBNE, K. & PAVLOVEC, R. 1991. Paleocene and Eocene beds in Slovenia and Istria. Introduction to the Paleogene SW Slovenia and Istria. Field and guidebook IGCP Project 286 “Early Paleogene Benthos”, Second Meeting, pp 7–17.
- DUPRAZ, C., REID, R.P., BRAISSANT, O., DECHO, A.W., NORMAN, R.S. & VISSER, P.T. 2009. Processes of carbonate precipitation in modern microbial mats. *Earth-Science Reviews* **96**, 141–162.
- EICKHOFF, M., BIRGEL, D., TALBOT, H.M., PECKMANN, J. & KAPPLER, A. 2013. Bacterioplanoid inventory of *Geobacter sulfurreducens* and *Geobacter metallireducens*. *Organic Geochemistry* **58**, 107–114.
- ELVERT, M., SUESS, E. & WHITICAR, M.J. 1999. Anaerobic methane oxidation associated with marine gas hydrates: superlight C-isotopes from saturated and unsaturated C₂₀ and C₂₅ irregular isoprenoids. *Naturwissenschaften* **86**, 295–300.
- ELVERT, M., BOETIUS, A., KNITTEL, K. & JØRGENSEN, B.B. 2003. Characterization of specific membrane fatty acids as chemotaxonomic markers for sulphate-reducing bacteria involved in anaerobic oxidation of methane. *Geomicrobiology Journal* **20**, 403–419.
- FENG, D., CHEN, D. & PECKMANN, J. 2009. Rare earth elements in seep carbonates as tracers of variable redox conditions at ancient hydrocarbon seeps. *Terra Nova* **21**, 49–56.
- GAILLARD, C., RIO, M. & ROLIN, Y. 1992. Fossil chemosynthetic communities related to vents or seeps in sedimentary basins: the pseudobioherms of southeastern France compared to other world examples. *Palaios* **7**, 451–465.
- GILL, F.L., HARDING, I.C., LITTLE, C.T.S. & TODD, J.A. 2005. Palaeogene and Neogene cold seep communities in Barbados, Trinidad and Venezuela: An overview. *Palaeogeography, Palaeoclimatology, Palaeoecology* **227**, 191–209.
- GOEDERT, J.L. & SQUIRES, R.L. 1990. Eocene deep-sea communities in localized limestones formed by subduction-related methane seeps, southwestern Washington. *Geology* **18**, 1182–1185.
- GOEDERT, J.L. & KALER, K.L. 1996. A new species of *Abyssochryso* (Gastropoda: Loxonematoidea) from a Middle Eocene cold-seep carbonate in the Humptulips Formation, western Washington. *The Veliger* **39**, 65–70.
- GOHRBANDT, K., KOLLMANN, K., KÜPPER, H., PAPP, A., PREY, S., WIESENEDER, H. & WOLETZ, G. 1960. Beobachtungen im Flysch von Triest. *Verhandlungen der Geologischen Bundesanstalt* **1960**, 162–196.
- GREINERT, J., BOHRMANN, G. & ELVERT, M. 2002. Stromatolitic fabric of authigenic carbonate crusts: result of anaerobic methane oxidation at cold seeps in 4,850 m water depth. *International Journal of Earth Sciences* **91**, 698–711.
- HAAS, A., PECKMANN, J., ELVERT, M., SAHLING, H. & BOHRMANN, G. 2010. Patterns of carbonate authigenesis at the Kouilou pockmarks on the Congo deep-sea fan. *Marine Geology* **268**, 129–136.
- HIMMLER, T., BRINKMANN, F., BOHRMANN, G. & PECKMANN, J. 2011. Corrosion patterns of seep-carbonates from the eastern Mediterranean Sea. *Terra Nova* **23**, 206–212.

- IADANZA, A., SAMPALMIERI, G., CIPOLLARI, P., MOLA, M. & COSENTINO, D. 2013. The “Brecciated Limestones” of Maiella, Italy: Rheological implications of hydrocarbon-charged fluid migration in the Messinian Mediterranean Basin. *Palaeogeography, Palaeoclimatology, Palaeoecology* **390**, 130–147.
- KIEL, S. 2008. An unusual new gastropod genus from an Eocene hydrocarbon seep in Washington State, USA. *Journal of Paleontology* **82**, 188–191.
- KIEL, S. 2010. The fossil record of vent and seep mollusks. In *The Vent and Seep Biota. Topics in Geobiology* (Ed S.Kiel), pp. 255–278. Heidelberg: Springer.
- KIEL, S., 2013. Lucinid bivalves from ancient methane seeps. *Journal of Molluscan Studies* **79**, 346–363.
- KIEL, S. & LITTLE, C.T.S., 2006. Cold seep mollusks are older than the general marine mollusk fauna. *Science* **313**, 1429–1431.
- KIEL, S. & PECKMANN, J. 2007. Chemosymbiotic bivalves and stable carbon isotopes indicate hydrocarbon seepage at four unusual Cenozoic fossil localities. *Lethaia* **40**, 345–357.
- KIEL, S. & AMANO, K., 2013. The earliest bathymodiolin mussels: Evaluation of Eocene and Oligocene taxa from deep-sea methane seep deposits in western Washington State, USA. *Journal of Paleontology* **87**, 589–602.
- KNITTEL, K. & BOETIUS, A. 2009. Anaerobic oxidation of methane: Progress with an unknown process. *Annual Review of Microbiology* **63**, 311–334.
- KRAUSE, S., ALOISI, G., ENGEL, A., LIEBETRAU, V. & TREUDE, T. 2014. Enhanced calcite dissolution in the presence of the aerobic methanotroph *Methylosinus trichosporium*. *Geomicrobiology Journal* **31**, 325–337.
- LORION, J., KIEL, S., FAURE, B.M., MASARU, K., HO, S.Y.W., MARSHALL, B.A., TSUCHIDA, S., MIYAZAKI, J.-I. & FUJIWARA, Y. 2013. Adaptive radiation of chemosymbiotic deep-sea mussels. *Proceedings of the Royal Society B* **280**, 20131243.
- LUCENTE, C.C. & TAVIANI, M. 2005. Chemosynthetic communities as fingerprints of submarine sliding-linked hydrocarbon seepage, Miocene deep-sea strata of the Tuscan–Romagna Apennines, Italy. *Palaeogeography, Palaeoclimatology, Palaeoecology* **227**, 176–190.
- LUFF, R. & WALLMANN, K. 2003. Fluid flow, methane fluxes, carbonate precipitation and biogeochemical turnover in gas hydrate-bearing sediments at Hydrate Ridge, Cascadia Margin: Numerical modeling and mass balances. *Geochimica et Cosmochimica Acta* **67**, 3403–3421.
- LUO, C. & REITNER, J. 2014. First report of fossil “keratose” demosponges in Phanerozoic carbonates: preservation and 3-D reconstruction. *Naturwissenschaften* **101**, 467–477.
- MAJIMA, R., NOBUHARA, T. & KITAZAKI, T., 2005. Review of fossil chemosynthetic assemblages in Japan. *Palaeogeography, Palaeoclimatology, Palaeoecology* **227**, 86–123.
- MARINČIĆ, S., ŠPARICA, M., TUNIS, G., UCHMAN, A. 1996. The Eocene flysch deposits of the Istrian Peninsula in Croatia and Slovenia: regional, stratigraphic, sedimentological and ichnological analyses. *Annales* **9**, 139–156.
- MARTIRE, L., NATALICCHIO, M., PETREA, C.C., CAVAGNA, S., CLARI, P. & PIERRE, F. 2010. Petrographic evidence of the past occurrence of gas hydrates in the Tertiary Piedmont Basin (NW Italy). *Geo-Marine Letters* **30**, 461–476.
- MATIČEC, D. 1994. Neotectonic deformations in Western Istria, Croatia. *Geologia Croatica* **47**, 199–204.
- MATSUMOTO, R. 1990. Vuggy carbonate crust formed by hydrocarbon seepage on the continental shelf of Baffin Island, northeast Canada. *Geochemical Journal* **24**, 143–158.
- MOALIC, Y., DESBRUYÈRES, D., DUARTE, C.M., ROZENFELD, A.F., BACHRATY, C. & ARNAUD-HAOND, S. 2012. Biogeography revisited with network theory: Retracing the history of hydrothermal vent communities. *Systematic Biology* **61**, 127–137.

- 624 NATALICCHIO, M., BIRGEL, D., DELA PIERRE, F., MARTIRE, L., CLARI, P., SPÖTL, C. &
625 PECKMANN, J. 2012. Polyphasic carbonate precipitation in the shallow subsurface:
626 Insights from microbially-formed authigenic carbonate beds in upper Miocene
627 sediments of the Tertiary Piedmont Basin (NW Italy). *Palaeogeography,*
628 *Palaeoclimatology, Palaeoecology* **329-330**, 158–172.
- 629 NATALICCHIO, M., DELA PIERRE, F., CLARI, P., BIRGEL, D., CAVAGNA, S., MARTIRE, L. &
630 PECKMANN, J. 2013. Hydrocarbon seepage during the Messinian salinity crisis in the
631 Tertiary Piedmont Basin (NW Italy). *Palaeogeography, Palaeoclimatology,*
632 *Palaeoecology* **390**, 68–80.
- 633 NAUHAUS, K., TREUDE, T., BOETIUS, A. & KRÜGER, M. 2005. Environmental regulation of the
634 anaerobic oxidation of methane: a comparison of ANME-1 and ANME-2 communities.
635 *Environmental Microbiology* **7**, 98–106.
- 636 NIEMANN, H. & ELVERT, M. 2008. Diagnostic lipid biomarker and stable carbon isotope
637 signatures of microbial communities mediating the anaerobic oxidation of methane with
638 sulphate. *Organic Geochemistry* **38**, 1668–1677.
- 639 OLU-LE ROY, K., SIBUET, M., FIALA-MÉDONI, A., GOFAS, S., SALAS, C., MARIOTTI, A.,
640 FOUCHER, J.-P. & WOODSIDE, J. 2004. Cold seep communities in the deep eastern
641 Mediterranean Sea: composition, symbiosis and spatial distribution on mud volcanoes.
642 *Deep-Sea Research I* **51**, 1915–1936.
- 643 PAVŠIČ, J. & PECKMANN J. 1996. Stratigraphy and sedimentology of the Piran Flysch Area
644 (Slovenia). *Annales* **9**, 123–138.
- 645 PAULL, C.K., HECKER, B., COMMEAU, R., FREEMAN-LYNDE, R.P., NEUMANN, C., GOLUBIC, S.,
646 HOOK, J.E., SIKES, E. & CURRAY, J. 1984. Biological communities at the Florida
647 Escarpment resemble hydrothermal vent taxa. *Science* **226**, 965–967.
- 648 PAULL, C.K., JULL, A.J.T., TOOLIN, L.J. & LINICK, T. 1985. Stable isotope evidence for
649 chemosynthesis in an abyssal seep community. *Nature* **317**, 709–711.
- 650 PAULL, C.K., CHANTON, J.P., NEUMANN, A.C., COSTON, J.A., MARTENS, C.S. & SHOWERS, W.
651 1992. Indicators of methane-derived carbonates and chemosynthetic organic carbon
652 deposits; examples from the Florida Escarpment. *Palaios* **7**, 361–375.
- 653 PECKMANN, J. & THIEL, V. 2004. Carbon cycling at ancient methane-seeps. *Chemical*
654 *Geology* **205**, 443–467.
- 655 PECKMANN, J., BIRGEL, D. & KIEL, S. 2009. Molecular fossils reveal fluid composition and
656 flow intensity at a Cretaceous seep. *Geology* **37**, 847–850.
- 657 PECKMANN, J., THIEL, V., MICHAELIS, W., CLARI, P., GAILLARD, C., MARTIRE, L. & REITNER,
658 J. 1999. Cold seep deposits of Beauvoisin (Oxfordian; southeastern France) and
659 Marmorito (Miocene; northern Italy): microbially induced authigenic carbonates.
660 *International Journal of Earth Sciences* **88**, 60–75.
- 661 PECKMANN, J., GOEDERT, J.L., HEINRICHS, T., HOEFS, J. & REITNER, J. 2003. The Late Eocene
662 'Whiskey Creek' methane-seep deposit (Western Washington State). *Facies* **48**, 223–
663 239.
- 664 PECKMANN, J., THIEL, V., REITNER, J., TAVIANI, M., AHARON, P. & MICHAELIS, W. 2004. A
665 microbial mat of a large sulfur bacterium preserved in a Miocene methane-seep
666 limestone. *Geomicrobiology Journal* **21**, 247–255.
- 667 PECKMANN, J., SENOWBARI-DARYAN, B., BIRGEL, D. & GOEDERT, J.L. 2007. The crustacean
668 ichnofossil *Palaxius* associated with callianassid body fossils in an Eocene methane-
669 seep limestone, Humptulips Formation, Olympic Peninsula, Washington. *Lethaia* **40**,
670 273–280.
- 671 REITNER, J., GAUTRET, P., MARIN, F. & NEUWEILER, F. 1995. Automicrites in modern marine
672 microbialite. Formation model via organic matrices (Lizard Island, Great Barrier Reef,
673 Australia). Bulletin de l'Institut Océanographique (Monaco) Numéro Spécial 14, 237–
674 264.

- REITNER, J., THIEL, V., ZANKL, H., MICHAELIS, W., WÖHRHEIDE, G. & GAUTRET P. 2000. Organic and biogeochemical patterns in cryptic microbialites. In *Microbial Sediments* (eds R.E. Riding & S. M. Awramik), pp.149–160. Berlin, Heidelberg: Springer Verlag.
- RICCI LUCCHI, F. & VAI, G.B. 1994. A stratigraphic and tectonofacies framework of the "calcarei a *Lucina*" in the Apennine Chain, Italy. *Geo-Marine Letters* **14**, 210–218.
- RIGBY, J.K. & GOEDERT, J.L. 1996. Fossil sponges from a localized cold-seep limestone in Oligocene rocks of the Olympic peninsula, Washington. *Journal of Paleontology* **70**, 900–908.
- RITGER, S., CARSON, B. & SUESS, E. 1997. Methane-derived authigenic carbonates formed by subduction-induced pore-water expulsion along the Oregon/Washington margin. *Geological Society of America Bulletin* **98**, 147–156.
- RITT, B., SARRAZIN, J., CAPRAIS, J.-C., NOËL, P., GAUTHIER, O., PIERRE, C., HENRY, P. & DESBRUYÈRES, D. 2010. First insights into the structure and environmental setting of cold-seep communities in the Marmara Sea. *Deep-Sea Research I* **57**, 1120–1136.
- RODRIGUES, C.F., DUPERRON, S. & GAUDRON, S.M. 2011. First documented record of a living solemyid bivalve in a pockmark of the Nile Deep-sea Fan (eastern Mediterranean Sea). *Marine Biodiversity Records*, 4: e10.
- ROSSELL, P.E., ELVERT, M., RAMETTE, A., BOETIUS, A. & HINRICHS, K.-U. 2011. Factors controlling the distribution of anaerobic methanotrophic communities in marine environments: Evidence from intact polar membrane lipids. *Geochimica et Cosmochimica Acta* **75**, 164–184.
- ROTERMAN, C.N., COPLEY, J.T., LINSE, K., TYLER, P.A. & ROGERS, A.D. 2013. The biogeography of the yeti crabs (Kiwaidae) with notes on the phylogeny of the Chirostyloidea (Decapoda: Anomura). *Proceedings of the Royal Society B* **280**, 20130718.
- SAHLING, H., RICKERT, D., LEE, R.W., LINKE, P. & SUESS, E. 2002. Macrofaunal community structure and sulfide flux at gas hydrate deposits from Cascadia convergent margin, NE Pacific. *Marine Ecology Progress Series* **231**, 121–138.
- SANDY, M.R., LAZĂR, I., PECKMANN, J., BIRGEL, D., STOICA, M. & ROBAN, R.D. 2012. Methane-seep brachiopod fauna within turbidites of the Sinaia Formation, Eastern Carpathian Mountains, Romania. *Palaeogeography, Palaeoclimatology, Palaeoecology* **323-325**, 42–59.
- SAUL, L.R., SQUIRES, R.L. & GOEDERT J.L. 1996. A new genus of cryptic lucinid? bivalve from Eocene cold seeps and turbidite-influenced mudstone, western Washington. *Journal of Paleontology* **70**, 788–794.
- SIBUET, M. & OLU, K. 1998. Biogeography, biodiversity and fluid dependence of deep-sea cold-seep communities at active and passive margins. *Deep-Sea Research II* **45**, 517–567.
- SQUIRES, R.L. & GOEDERT J.L. 1991. New Late Eocene mollusks from localized limestone deposits formed by subduction-related methane seeps, southwestern Washington. *Journal of Paleontology* **65**, 412–416.
- STILLER, J., ROUSSET, V., PLEIJEL, F., CHEVALDONNE, P., VRIJENHOEK, R.C. & ROUSE, G.W. 2013. Phylogeny, biogeography and systematics of hydrothermal vent and methane seep *Amphisamytha* (Ampharetidae, Annelida), with descriptions of three new species. *Systematics and Biodiversity* **11**, 35–65.
- TAVIANI, M. 1994. The "calcarei a *Lucina*" macrofauna reconsidered: Deep-sea faunal oases from Miocene-age cold vents in the Romagna Apennine, Italy. *Geo-Marine Letters* **14**, 185–191.
- TAVIANI, M. 2011. The deep-sea chemoautotroph microbial world as experienced by the Mediterranean metazoans through time. In *Advances in Stromatolite Geobiology*.

- 725 *Lecture Notes in Earth Sciences 131* (eds J. Reitner et al.), pp. 277–295. Berlin:
726 Springer.
- 727 TAVIANI, M. 2014. Marine chemosynthesis in the Mediterranean Sea. In *The Mediterranean*
728 *Sea: Its history and present challenges* (eds S. Goffredo & Z. Dubinsky), pp. 69–83.
729 Dordrecht: Springer.
- 730 TAVIANI, M., ANGELETTI, L. & CEREGATO, A. 2011. Chemosynthetic bivalves of the family
731 Solemyidae (Bivalvia, Protobranchia) in the Neogene of the Mediterranean Basin.
732 *Journal of Paleontology* **85**, 1067–1076.
- 733 TAVIANI, M., ANGELETTI, L., CEREGATO, A., FOGLINI, F., FROGLIA, C. & TRINCARDI, F. 2013.
734 The Gela Basin pockmark field in the strait of Sicily (Mediterranean Sea):
735 chemosymbiotic faunal and carbonate signatures of postglacial to modern cold seepage.
736 *Biogeosciences* **10**, 4653–4671.
- 737 TEICHERT, B.M.A. & VAN DE SCHOOTBRUGGE, B. 2013. Tracing Phanerozoic hydrocarbon
738 seepage from local basins to the global Earth system. *Palaeogeography,*
739 *Palaeoclimatology, Palaeoecology* **390**, 1–3.
- 740 THIEL, V., PECKMANN, J., SCHMALE, O., REITNER, J. & MICHAELIS, W. 2001. A new straight-
741 chain hydrocarbon biomarker associated with anaerobic methane cycling. *Organic*
742 *Geochemistry* **32**, 1019–1023.
- 743 TREUDE, T., KNITTEL, K., BLUMENBERG, M., SEIFERT, R. & BOETIUS, A. 2005. Subsurface
744 microbial methanotrophic mats in the Black Sea. *Applied and Environmental*
745 *Microbiology* **71**, 6375–6378.
- 746 TRIBOLLET, A., GOLUBIC, S., RADTKE, G. & REITNER, J. 2011. On microbiocorrosion. In
747 *Advances in Stromatolite Geobiology. Lecture Notes in Earth Sciences 131* (eds J.
748 Reitner et al.), pp. 265–276. Berlin: Springer.
- 749 VACELET, J., FIALA-MÉDIONI, A., FISHER, C.R. & BOURY-ESNAULT, N. 1996. Symbiosis
750 between methane oxidizing bacteria and a deep-sea carnivorous cladorhizid sponge.
751 *Marine Ecology Progress Series* **145**, 77–85.
- 752 VENTURINI, S., SELMO, E., TARLAO, A. & TUNIS, G. 1998. Fossiliferous methanogenic
753 limestones in the Eocene flysch of Istria (Croatia). *Giornale di Geologia* **60**, 219–234.
- 754 VRIJENHOEK, R.C., 2013. On the instability and evolutionary age of deep-sea chemosynthetic
755 communities. *Deep-Sea Research II* **92**, 189–200.
- 756 ŽIVKOVIC, S. & BABIĆ, L. 2003. Paleoceanographic implications of smaller benthic and
757 planktonic foraminifera from the Eocene Pazin Basin (Coastal Dinarides, Croatia).
758 *Facies* **49**, 49–60.

1
2
3 761 **Figure and table captions:**

4
5 762 Figure 1. Working area. (a) Distribution of the main domains of Cenozoic seep deposits in the
6
7 763 Mediterranean area. (b) Geological sketch of the Istria region and location of the Buje seep
8
9 764 deposits (45°24'31''N, 13°40'01''E).

10
11 765
12
13
14 766 Figure 2. Composite image of studied Buje 1 to 3 seep deposits assembled from three
15
16 767 photographs.

17
18 768
19
20
21 769 Figure 3. Outcrop photographs of the studied seep carbonates. (a) Buje 1 and 2 seep deposits;
22
23 770 person for scale. Note that the Buje 1 seep deposit is faintly stratified. (b) The lenticular Buje
24
25 771 3 seep deposit; hammer for scale.

26
27 772
28
29 773 Figure 4. Bivalves from the Buje 1 seep deposit. (a-c) The solemyid *Acharax*; (a) large
30
31 774 specimen ([GZG.INV.82757](#)), (b) detail showing the S-shaped band on the anterodorsal shell
32
33 775 margin (arrow), and (c) small fragment showing radial ribs on the anterior part of the shell
34
35 776 ([GZG.INV.82758](#)). (d) The protobranch *Nucula* ([GZG.INV.82759](#)). (e) Large specimen of
36
37 777 *Thyasira* showing the posterior sulcus ([GZG.INV.82760](#)). (f-j) The lucinid *Amanocina*; (f)
38
39 778 specimen with naticid drill hole (arrow; [GZG.INV.82761](#)); (g,h) specimen showing the
40
41 779 narrow escutcheon ([GZG.INV.82762](#)); (i,j) large specimen ([GZG.INV.82763](#)) in dorsal view
42
43 780 (i) and view on the edentulous hinge (j).

44
45 781
46
47
48
49 782 Figure 5. Scanned thin sections of the three Buje seep deposits: (a) Buje 1, (b) Buje 2 (c) Buje
50
51 783 3. The limestones represent bioturbated mudstone and wackestone; arrows indicate geopetal
52
53 784 cavities (a) and black corrosion rims (c).

54
55 785
56
57
58
59
60

Figure 6. Petrography of Buje seep deposits. m – matrix micrite; pm – peloidal micrite; ccc – circumgranular calcite cement; bbc – banded and botryoidal cement; s – sediment; ec – equant calcite cement. (a) Angular clasts cemented by matrix micrite, plane-polarized light. (b) Same detail as (a) showing the brightly fluorescent micrite; fluorescence image. (c) Fossiliferous wackestone containing planktic (white arrows) and benthic (black arrows) foraminifera; plane-polarized light. (d-f) Irregular cavities filled with peloidal micrite, sediment, and different generations of carbonate cements; plane-polarized light.

Figure 7. Petrography of cauliflower micrite. m – matrix micrite; pm – peloidal micrite; ccc – circumgranular calcite cement; cm – cauliflower micrite; ec – equant calcite cement. (a) Domal and grooved cauliflower micrite that grew on peloidal micrite and was postdated by circumgranular calcite and equant calcite cement, plane-polarized light. (b) Detail of (a). (c) Close up view of the cauliflower micrite with internal reticulate porosity filled by microspar (arrows); crossed-polarized light. (d) The cauliflower micrite exhibits an intense autofluorescence; fluorescence image.

Figure 8. Corrosion patterns. m – matrix micrite; bbc – banded and botryoidal cement; s – sediment. (a) Highly irregular cavity surface covered by a black rim (arrows); plane-polarized light. (b) Close up view of the dark irregular rim (arrow); plane-polarized light. (c) Bright spots on corrosion surfaces reveal an enrichment in iron (Fe) and manganese (Mn); see inserted EDS spectrum; SEM micrograph of thin section, backscatter view.

Figure 9. Cross plot of the carbon and oxygen stable isotope compositions in per mil versus VPDB standard of micrite forming the Buje seep deposits.

1
2
3
4
5
6
7
8
9
10
11
12
13
14
15
16
17
18
19
20
21
22
23
24
25
26
27
28
29
30
31
32
33
34
35
36
37
38
39
40
41
42
43
44
45
46
47
48
49
50
51
52
53
54
55
56
57
58
59
60

Figure 10. Lipid biomarker patterns of the Buje 1 seep deposit; numbers in italics indicate compound-specific $\delta^{13}\text{C}$ values in per mil versus VPDB standard. Gas chromatograms (total ion current) of hydrocarbon (a) and carboxylic acid (b) fractions. (a) Circles – *n*-alkanes; white triangles – regular, head-to-tail linked isoprenoids; black triangles – irregular, tail-to-tail linked isoprenoids; grey triangles – irregular, head-to-head linked isoprenoids (biphytanes); Cr – crocetane; Ph – phytane; PMI – pentamethylicosane; Sq – squalane; black squares – steranes; istd – internal standard. (b) Circles – *n*-fatty acids; *i* – *iso*-fatty acids; *ai* – *anteiso*-fatty acids; M – monoenoic fatty acids; white triangles – regular, head-to-tail linked isoprenoidal acids; PMI – pentamethylicosanoic acid; $\beta\beta$ -32-HA – *17 β (H),21 β (H)-bishomohopanoic acid*; istd – internal standard.

822 Table 1. Schematic overview of the Palaeogene and Neogene seep deposits across the Mediterranean

Locality	Age	Type of seep	Fossil assemblage	$\delta^{13}\text{C}$ [‰VPDB]	$\delta^{18}\text{O}$ [‰VPDB]	References
Emilian Apennine (Italy)	Early Pliocene	Fossiliferous limestones, conduits	Solemyids and lucinids	-25 to -17	-3 to +3	Taviani <i>et al.</i> 1997; Barbieri and Cavalazzi, 2005
Tortona Apennine (Piedmont, Italy)	Late Miocene	<i>Lucina</i> and brecciated limestones, carbonate beds with veins, conduits	Lucinids, tubeworms, bacterial biofilms	-56 to +6	-6 to +7	Dela Pierre <i>et al.</i> 2010; Martire <i>et al.</i> 2010; Natalicchio <i>et al.</i> 2012, 2013
Maiella, central Apennine (Italy)	Late Miocene	Brecciated limestones	absent	-40 to +4	-9 to +4	Iadanza <i>et al.</i> 2013
Monferrato (Piedmont, Italy)	Middle and Late Miocene	<i>Lucina</i> and brecciated limestones, macroconcretions with veins, conduits	Lucinids, tubeworms, bacterial biofilms	-45 to -9	-1 to 8	Clari <i>et al.</i> 1988, 1994, 2009; Peckmann <i>et al.</i> 1999
Sicily (Italy)	Middle and Late Miocene	<i>Lucina</i> and brecciated limestones	Lucinids (?)	-49 to -29	+3 to +9	Ricci Lucchi and Vai, 1994
Tuscan-Romagna Apennine (Italy)	Early and Late Miocene	Fossiliferous and brecciated limestones	Solemyids, lucinids, bathymodiolins, and vesicomys	-58 to -16	-5 to +5	Taviani <i>et al.</i> 1997; Conti and Fontana, 1999, 2005; Lucente and Taviani, 2005
Buje (Croatia)	Middle Eocene	Fossiliferous limestones	Solemyids (<i>Acharax</i>), thysirids (<i>Thyasira</i>), lucinids (<i>Amanocina</i>), nukulids, <i>Callianassa</i>	-42 to -23	-4 to 0	Venturini <i>et al.</i> 1998; this study

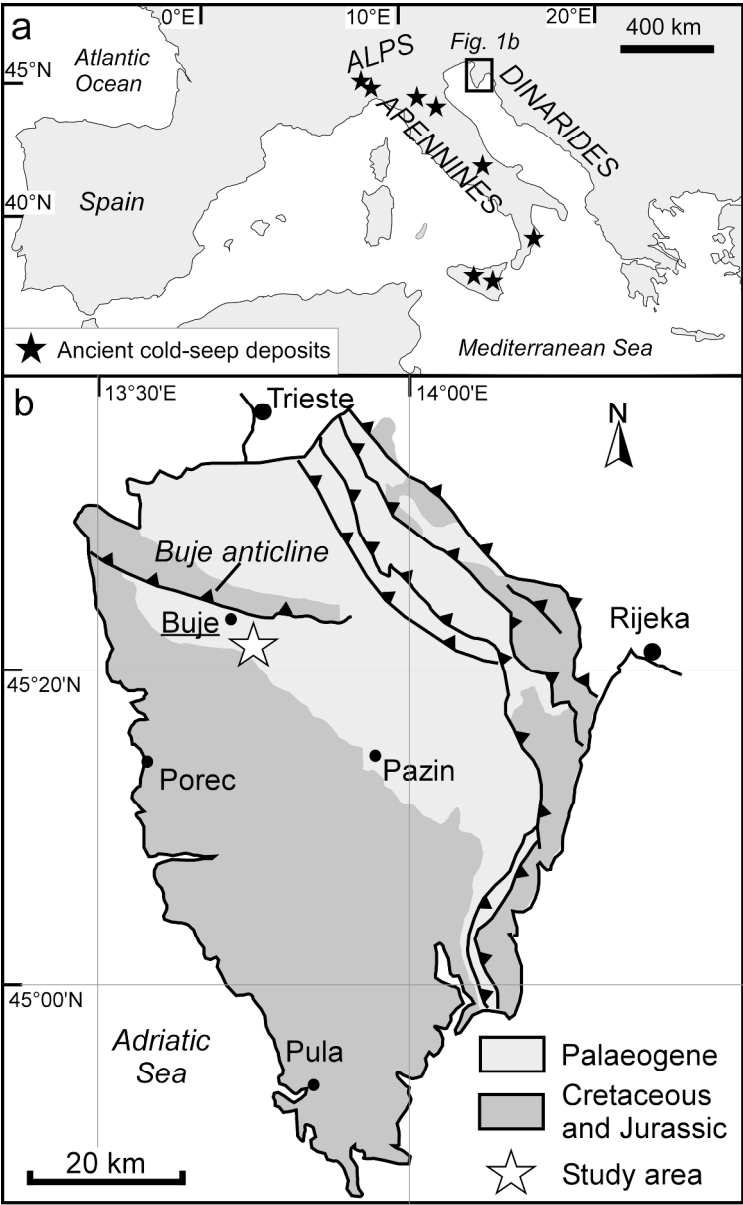


Figure 1. Working area. (a) Distribution of the main domains of Cenozoic seep deposits in the Mediterranean area. (b) Geological sketch of the Istria region and location of the Buje seep deposits (45°24'31"N, 13°40'01"E).
129x208mm (600 x 600 DPI)



Figure 2. Composite image of studied Buje 1 to 3 seep deposits assembled from three photographs.
48x14mm (300 x 300 DPI)

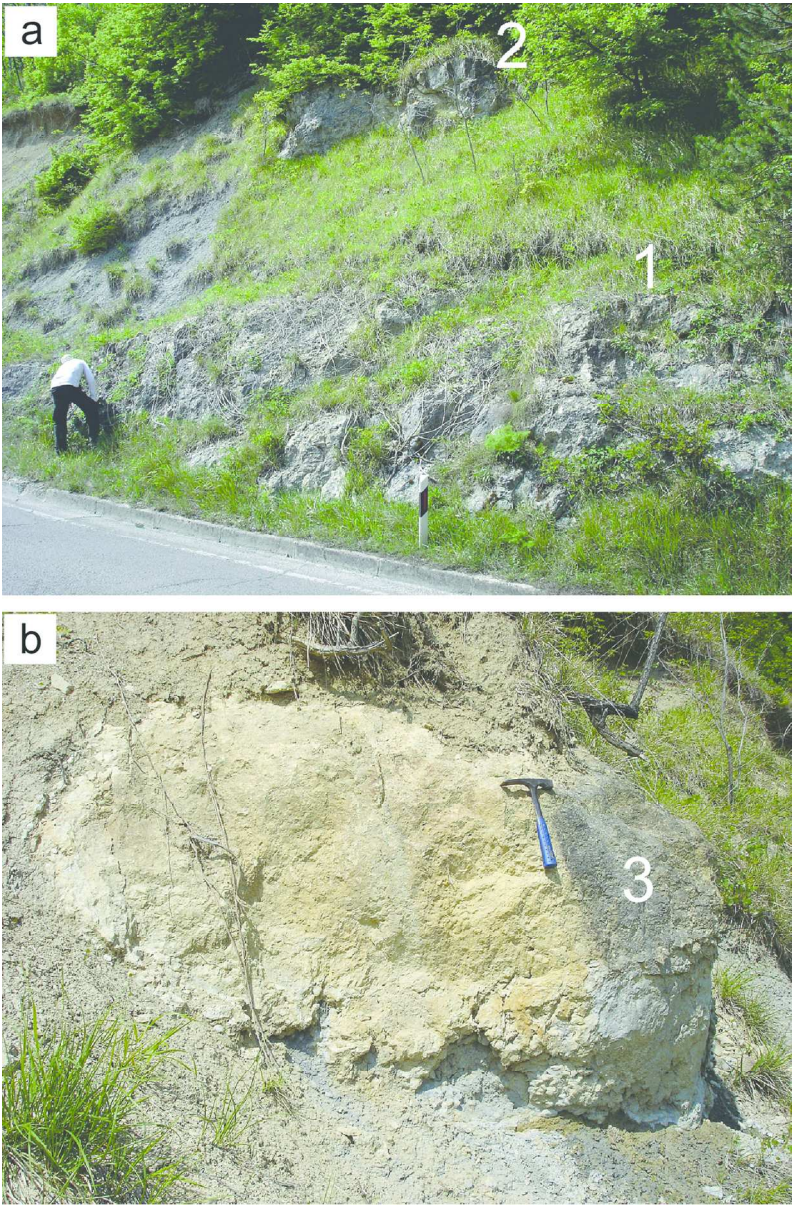


Figure 3. Outcrop photographs of the studied seep carbonates. (a) Buje 1 and 2 seep deposits; person for scale. Note that the Buje 1 seep deposit is faintly stratified. (b) The lenticular Buje 3 seep deposit; hammer for scale.
121x185mm (300 x 300 DPI)

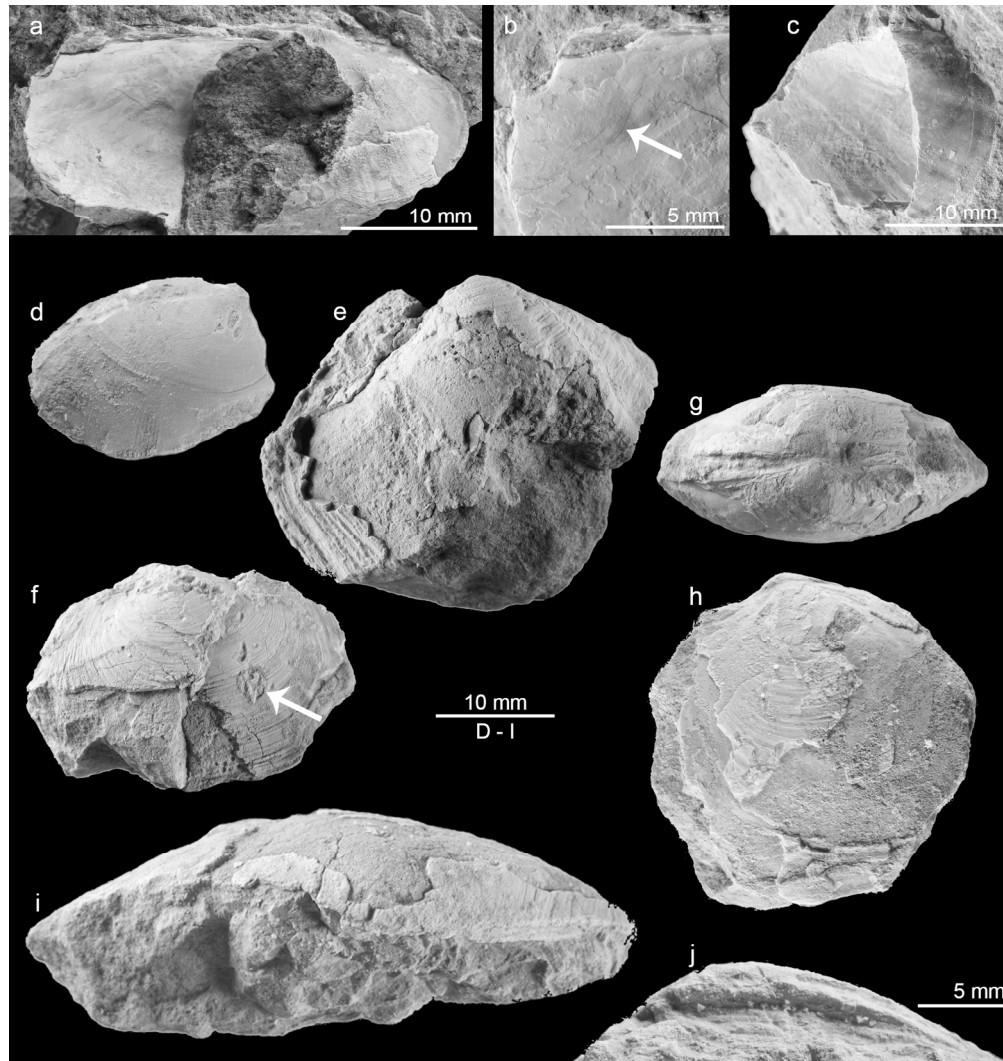


Figure 4. Bivalves from the Buje 1 seep deposit. (a-c) The solemyid *Acharax*; (a) large specimen (GZG.INV.82757), (b) detail showing the S-shaped band on the anterodorsal shell margin (arrow), and (c) small fragment showing radial ribs on the anterior part of the shell (GZG.INV.82758). (d) The protobranch *Nucula* (GZG.INV.82759). (e) Large specimen of *Thyasira* showing the posterior sulcus (GZG.INV.82760). (f-j) The lucinid *Amanocina*; (f) specimen with naticid drill hole (arrow; GZG.INV.82761); (g, h) specimen showing the narrow escutcheon (GZG.INV.82762); (i, j) large specimen (GZG.INV.82763) in dorsal view (i) and view on the edentulous hinge (j).
168x178mm (300 x 300 DPI)

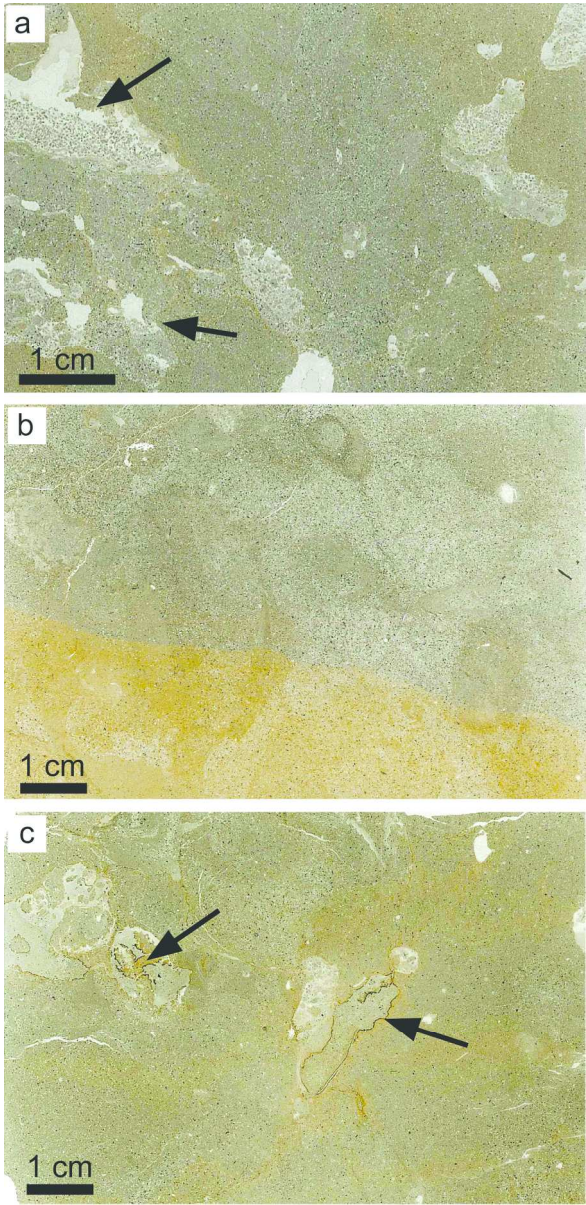


Figure 5. Scanned thin sections of the three Buje seep deposits: (a) Buje 1, (b) Buje 2 (c) Buje 3. The limestones represent bioturbated mudstone and wackestone; arrows indicate geopetal cavities (a) and black corrosion rims (c).
165x341mm (300 x 300 DPI)

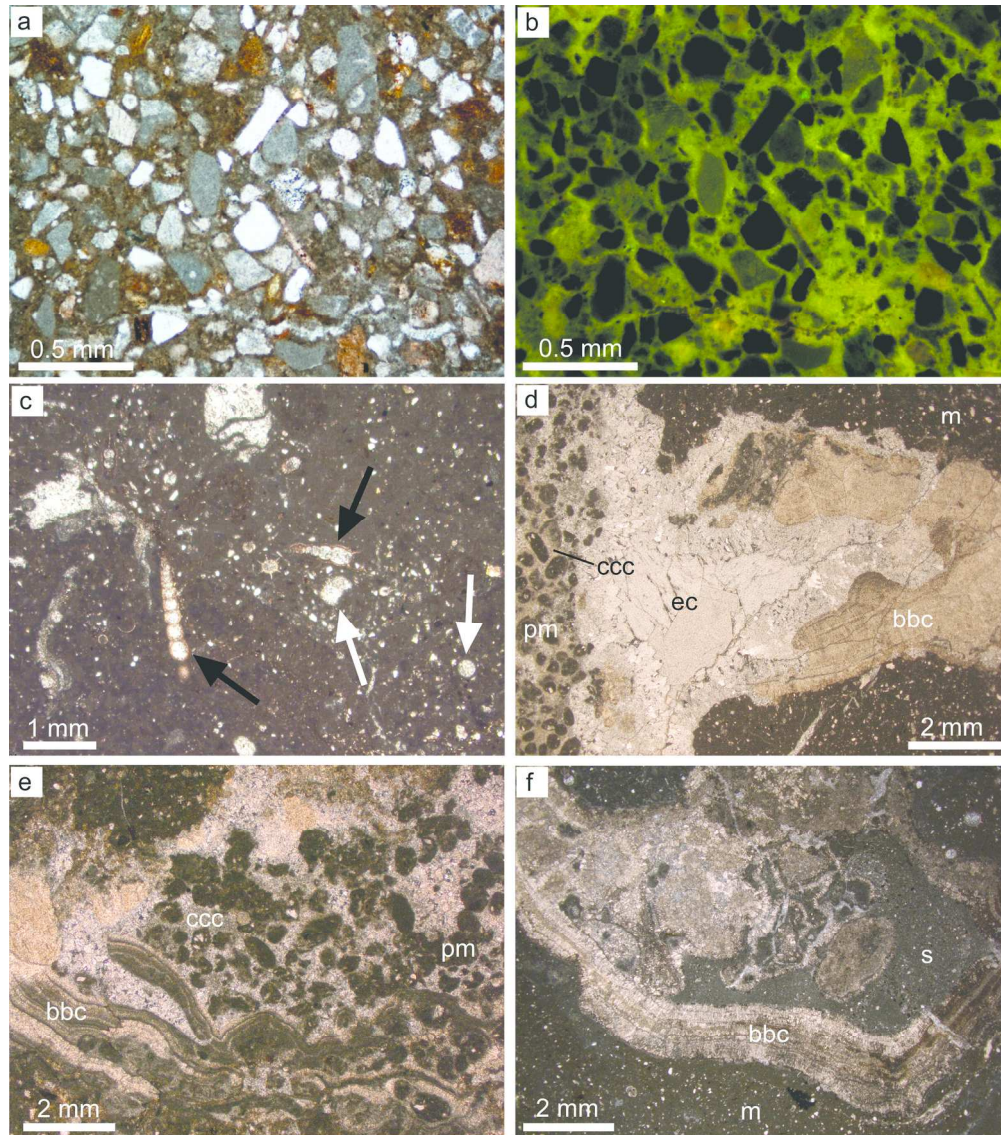


Figure 6. Petrography of Buje seep deposits. m – matrix micrite; pm – peloidal micrite; ccc – circumgranular calcite cement; bbc – banded and botryoidal cement; s – sediment; ec – equant calcite cement. (a) Angular clasts cemented by matrix micrite, plane-polarized light. (b) Same detail as (a) showing the brightly fluorescent micrite; fluorescence image. (c) Fossiliferous wackestone containing planktic (white arrows) and benthic (black arrows) foraminifera; plane-polarized light. (d-f) Irregular cavities filled with peloidal micrite, sediment, and different generations of carbonate cements; plane-polarized light.

191x215mm (300 x 300 DPI)

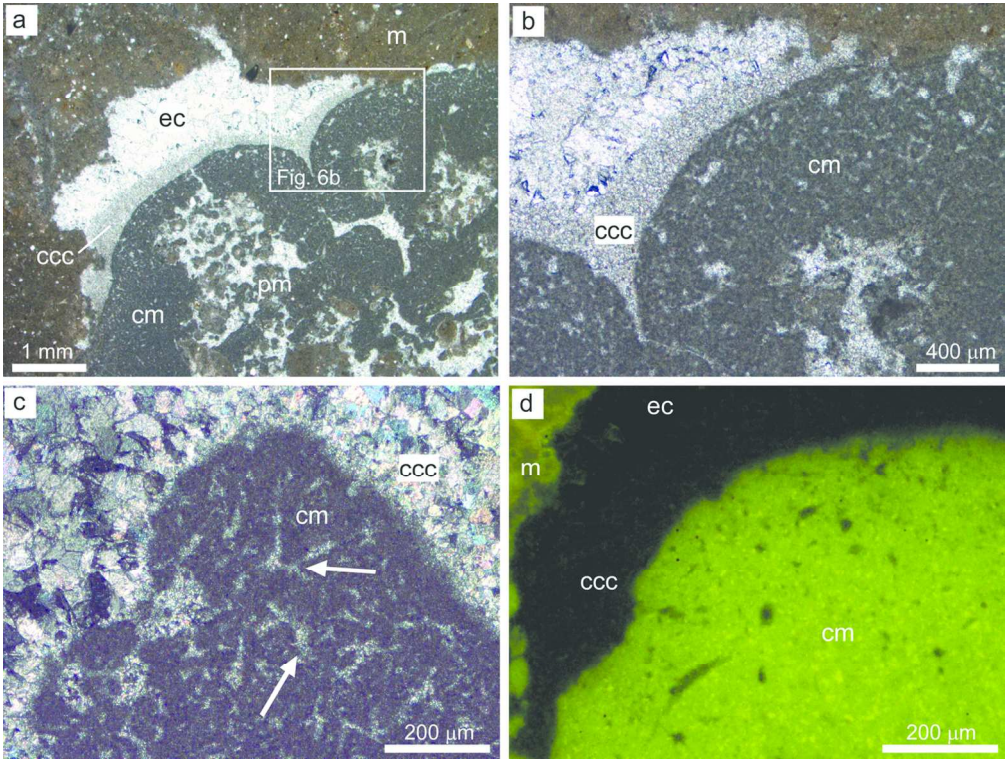


Figure 7. Petrography of cauliflower micrite. m – matrix micrite; pm – peloidal micrite; ccc – circumgranular calcite cement; cm – cauliflower micrite; ec – equant calcite cement. (a) Domal and grooved cauliflower micrite that grew on peloidal micrite and was postdated by circumgranular calcite and equant calcite cement, plane-polarized light. (b) Detail of (a). (c) Close up view of the cauliflower micrite with internal reticulate porosity filled by microspar (arrows); crossed-polarized light. (d) The cauliflower micrite exhibits an intense autofluorescence; fluorescence image.
127x96mm (300 x 300 DPI)

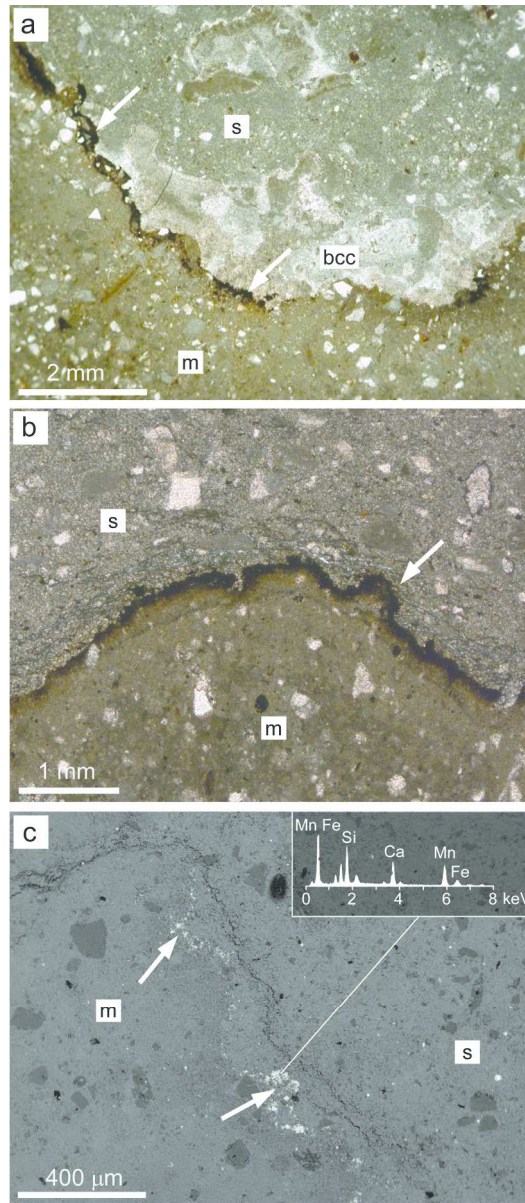


Figure 8. Corrosion patterns. m – matrix micrite; bbc – banded and botryoidal cement; s – sediment. (a) Highly irregular cavity surface covered by a black rim (arrows); plane-polarized light. (b) Close up view of the dark irregular rim (arrow); plane-polarized light. (c) Bright spots on corrosion surfaces reveal an enrichment in iron (Fe) and manganese (Mn); see inserted EDS spectrum; SEM micrograph of thin section, backscatter view.
182x416mm (300 x 300 DPI)

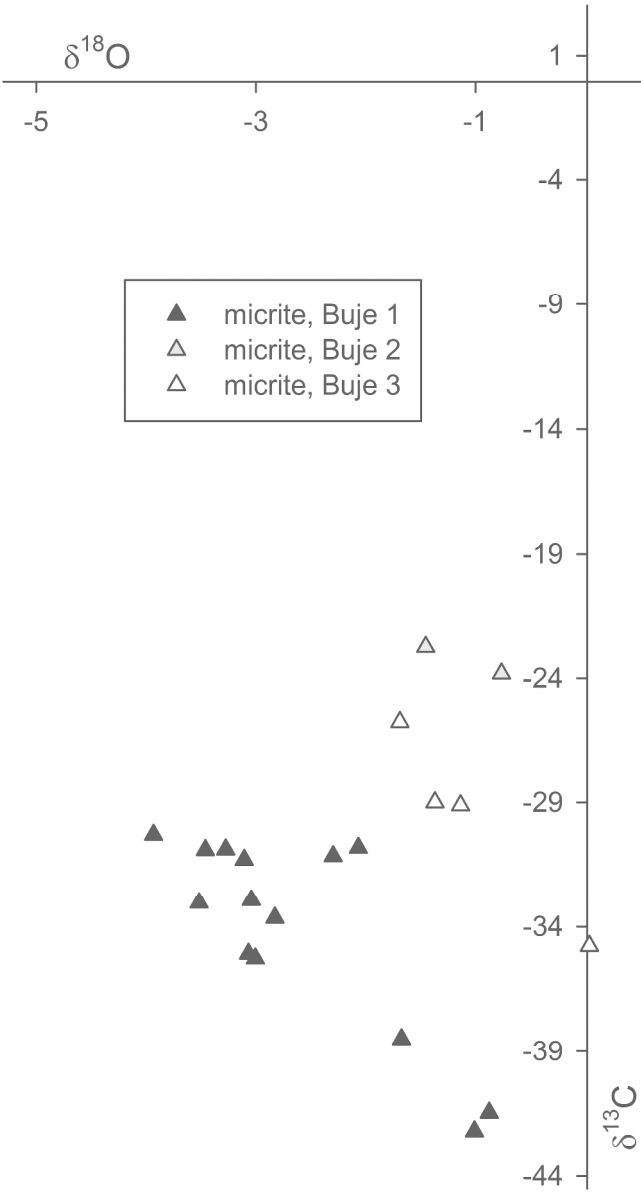


Figure 9. Cross plot of the carbon and oxygen stable isotope compositions in per mil versus VPDB standard of micrite forming the Buje seep deposits.
146x267mm (600 x 600 DPI)

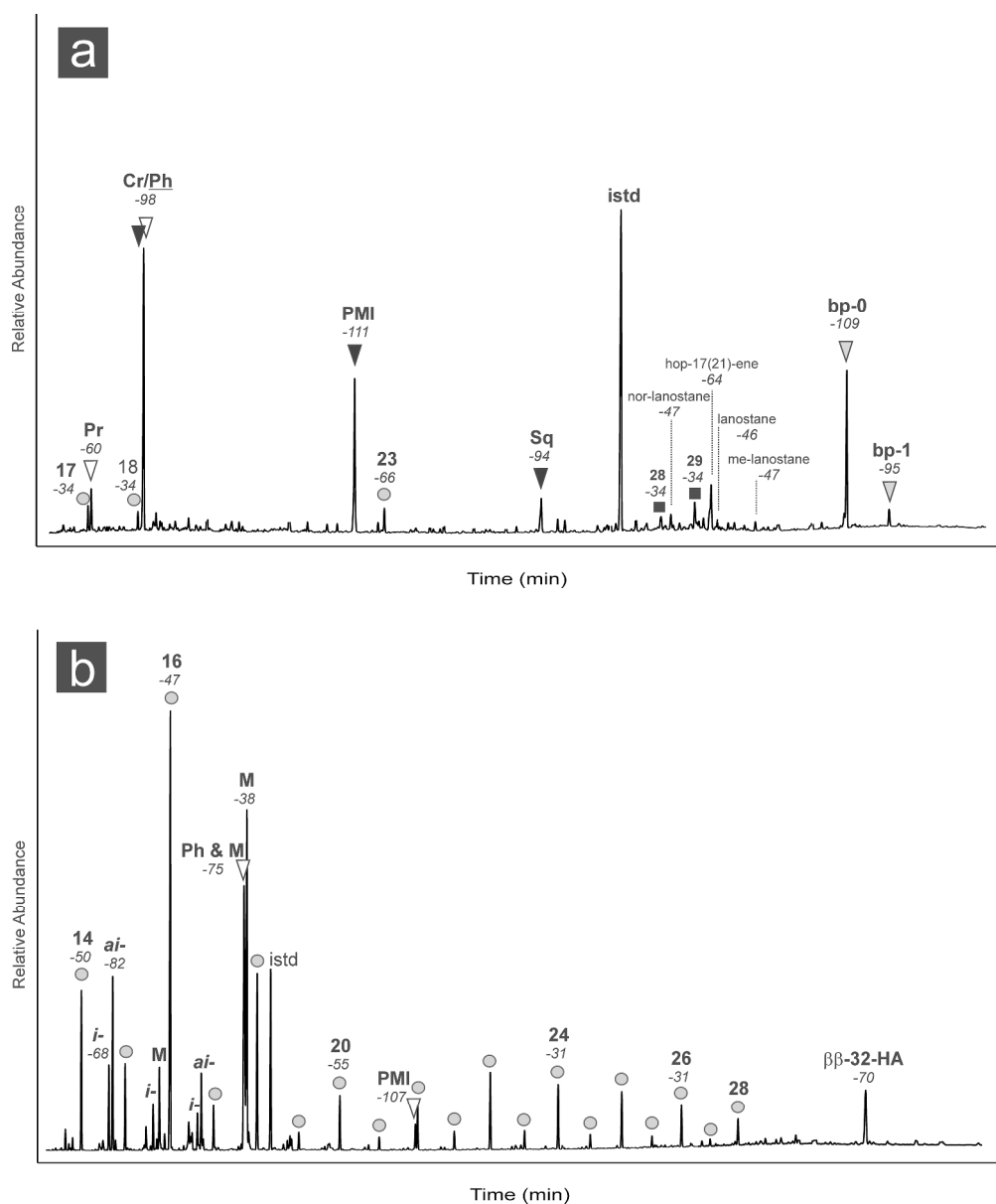


Figure 10. Lipid biomarker patterns of the Buje 1 seep deposit; numbers in italics indicate compound-specific $\delta^{13}C$ values in per mil versus VPDB standard. Gas chromatograms (total ion current) of hydrocarbon (a) and carboxylic acid (b) fractions. (a) Circles – n-alkanes; white triangles – regular, head-to-tail linked isoprenoids; black triangles – irregular, tail-to-tail linked isoprenoids; grey triangles – irregular, head-to-head linked isoprenoids (biphytanes); Cr – crocetane; Ph – phytane; PMI – pentamethylcosane; Sq – squalane; black squares – steranes; istd – internal standard. (b) Circles – n-fatty acids; i – iso-fatty acids; ai – anteiso-fatty acids; M – monoenoic fatty acids; white triangles – regular, head-to-tail linked isoprenoidal acids; PMI – pentamethylcosanoic acid; $\beta\beta$ -32-HA – 17 β (H),21 β (H)-bishomohopanoic acid; istd – internal standard.

202x241mm (600 x 600 DPI)